



저작자표시-비영리-변경금지 2.0 대한민국

이용자는 아래의 조건을 따르는 경우에 한하여 자유롭게

- 이 저작물을 복제, 배포, 전송, 전시, 공연 및 방송할 수 있습니다.

다음과 같은 조건을 따라야 합니다:



저작자표시. 귀하는 원저작자를 표시하여야 합니다.



비영리. 귀하는 이 저작물을 영리 목적으로 이용할 수 없습니다.



변경금지. 귀하는 이 저작물을 개작, 변형 또는 가공할 수 없습니다.

- 귀하는, 이 저작물의 재이용이나 배포의 경우, 이 저작물에 적용된 이용허락조건을 명확하게 나타내어야 합니다.
- 저작권자로부터 별도의 허가를 받으면 이러한 조건들은 적용되지 않습니다.

저작권법에 따른 이용자의 권리는 위의 내용에 의하여 영향을 받지 않습니다.

이것은 [이용허락규약\(Legal Code\)](#)을 이해하기 쉽게 요약한 것입니다.

[Disclaimer](#)

Doctoral Thesis

Development of Film type solid electrolyte for Na
ion solid-state battery using oxide ceramic -
polymer composite process

Young Jun Lim

Department of Energy Engineering
(Battery Science and Technology)

Graduate School of UNIST

2020

Development of Film type solid electrolyte for Na
ion solid-state battery using oxide ceramic -
polymer composite process

Young Jun Lim

Department of Energy Engineering
(Battery Science and Technology)

Graduate School of UNIST

Development of Film type solid electrolyte for Na
ion solid-state battery using oxide ceramic -
polymer composite process

A thesis/dissertation
submitted to the Graduate School of UNIST
in partial fulfillment of the
requirements for the degree of
Doctor of Philosophy

Young Jun Lim

06/02/2020 of submission

Approved by



Advisor

Youngsik Kim

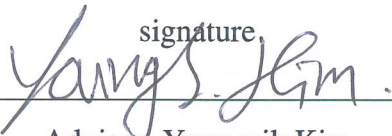
Development of Film type solid electrolyte for Na
ion solid-state battery using oxide ceramic -
polymer composite process

Young Jun Lim

This certifies that the thesis/dissertation of Young Jun Lim is
approved.


06/02/2020 of submission

signature



Advisor: Youngsik Kim

signature



Yunseok Choi

signature




Kyeong-Min Jeong

signature



Dongwoog Lee

signature



Jae-Kwang Kim

Abstract

Young Jun Lim

School of Energy and Chemical Engineering, UNIST

Advisor – Youngsik Kim

Demand for energy storage systems in mobile device, electric vehicles (EVs), large scale energy storage systems (ESSs), and other areas continues to grow. The Li-ion batteries (LIBs) have a high energy density among currently commercialized secondary batteries and have been continuously studied and applied to various fields. However, the demand for lithium-ion batteries continues to increase, while global supplies to lithium sources are limited. The research on next-generation materials that can replace lithium is underway. Na have good advantage for Na-ion batteries (NIBs) because of their abundance and low-cost effect. To emphasize these advantages of Na based chemical engineering, further study on electrode materials, electrolytes, and electrode-electrolyte interactions is required. In the case of the existing battery system, an organic liquid electrolyte is used, which always causes a problem of safety. Currently researched NIBs have several issues regarding their organic liquid electrolytes, including flammability and potential safety hazards in large-scale applications. In view of this safety issue, Na-ion solid-state battery systems that do not use organic liquid electrolytes are considered to be a suitable solution, and making solid electrolytes is important in the future of batteries.

In general, the solid electrolytes used to develop Na-ion solid state battery systems are based on inorganic solid materials; particularly, oxide-based materials that have high ionic conductivity and are electrochemically and thermally stable are being studied. $\text{Na}_3\text{Zr}_2\text{Si}_2\text{PO}_{12}$ (Na super ionic conductor, NASICON) solid electrolytes are the most promising oxide-based Na-ion conducting material, with a high ionic conductivity of over 10^{-4} S/cm at room temperature and stable air and moisture. NASICON ceramics are electrochemically stable up to 7 V, making it suitable for use in high voltage batteries. Owing to its stability advantages, efforts have been made to use NASICON in solid-state NIB systems. However, there remains a critical problem in the resistance between solid particle interfaces caused by the fragile and rigid nature of the oxide material itself, regardless of how high the pressure of the solid electrolyte powder is, making it difficult to utilize in a solid-state battery system.

There have been numerous studies on composite electrolytes with polymer materials with the aim to counteract the solid-solid interface resistance of these oxide-based solid particles. Polymer materials have flexible physical properties and are therefore suitable to compensate for the disadvantages of oxide-based solid ceramic electrolytes. In most of the studies that use Na-ion conducting ceramics, a composite electrolyte was prepared with the aim that the ceramic powder would fill the role of ion transport in the polymer electrolyte. If ion transfer through the ceramic is confirmed, it is possible to increase the ceramic ratio and expect a thermally and electrochemically stable composite. However, if

there is no ion transfer through the ceramic, the ionic conductivity decreases as the proportion of ceramics increases. According to a recent report, the ion conductivity in the abovementioned composite electrolyte exists primarily through the polymer electrolyte, and the ceramics contribution is negligible. Therefore, the ceramic is used only as a filler of the polymer electrolyte, and as the ratio of the polymer electrolyte is still high, the thermal and electrochemical instability characteristics of the polymer remain.

The influence of the solid electrolyte is not readily seen when the oxide ceramic is in a powder state. Therefore, more research is required surrounding methods that aim to increase the ceramic proportion and enable ion transport through ceramics. In particular, for ion conduction through ceramics, the ion transport channel of the oxide-based solid electrolyte must be formed separately in the composite electrolyte.

In this study, we propose a top-down method of combining a polymer with a ceramic in which an ion transfer channel has been previously formed. This allows for the main ion transport channel to pass through the ceramic while the polymer material can be used to improve the physical properties of the solid electrolyte. Moreover, since the proportion of ceramic in the composite electrolyte occupies more than 50 wt%, a thermally and electrochemically stable solid electrolyte can be produced.

To confirm the possibility of a top-down composite electrolyte, we used a method of partially sintering a high porosity ceramic solid electrolyte and filling its internal pores with a polymer material to increase the physical strength. A NASICON ceramic solid electrolyte was used as the oxide-based solid electrolyte, and epoxy-NASICON solid electrolyte pellets were prepared by filling the internal pores with an epoxy-resin polymer material, thereby confirming the possibility of using the electrolyte in an NIB. Through this method, the physical properties are expected to increase in strength owing to the use of epoxy-resin polymer materials, while the ion conduction effect can be transferred through the sintered NASICON solid ceramic to create a high stable solid ceramic electrolyte. As a result, the ionic conductivity becomes 1.45×10^{-4} S/cm, the thermal and electrochemical stability of NASICON is maintained, and the physical strength is enhanced by approximately 2 times more than that of the bare NASICON pellet. In addition, cell performance stability of 20 cycles were confirmed in a half-cell with a $\text{Na}_3\text{V}_2(\text{PO}_4)_3$ (NVP) cathode and Na metal. After confirming the composite possibility of the sintered oxide-based solid electrolyte and the polymer material through the existing ceramic pellet form, a thinner and more flexible film-type solid electrolyte was intended to be produced. To this end, the existing ceramic solid electrolyte sintering was sintered in a specific pattern to form an ion transfer channel and to have physical strength. Currently, the method of sintering by simply compressing the powder has a characteristic that the ion transfer channel of the ceramic after sintering is random and still breaks easily. If it can be made into a specific shape, the ion transport channel can be optimized, and a ceramic solid electrolyte can be produced in a form that is not easily broken physically. Patterned sintering can be easily accomplished by impregnating a ceramic solid electrolyte solution using a

template with a specific shape, followed by sintering. Thus, a solid electrolyte membrane in the form of a thinner and more flexible film was made by combining a ceramic solid electrolyte patterned with a specific shape and a polymer material. The final solid electrolyte film shows an ionic conductivity of 1.04×10^{-4} S/cm and shows stable characteristics of 20 cycles in a $\text{Na}_3\text{V}_2(\text{PO}_4)_3$ cathode and Na metal half-cell test. This method will suggest a new direction to the existing method for producing a composite electrolyte using an oxide-based solid electrolyte. It is expected that composite solid electrolytes may be applied to various battery systems by combining the oxide-based solid electrolyte and the polymer material.

Contents

Abstract	i
List of Figures	iv
List of Tables	viii
I. Introduction and Background	1
1.1. Basic principle of Li ion and Na-ion battery system	1
1.2. Current safety issue of organic liquid electrolyte	4
1.3. All-solid-state battery system for Na-ion batteries	4
2.3.1 Solid electrolyte for all-solid-state batteries	4
2.3.2 Properties of Oxide ceramic solid electrolytes	4
2.3.3 Current research trend of Oxide ceramic solid electrolyte	7
II. Experimental	16
2.1. Preparation of materials	16
2.2. Preparation of solid electrolytes and electrodes	17
2.3. Material characterization	17
III. Results and Discussion	19
3.1. Epoxy-NASICON solid electrolyte pellet after sintering process	19
3.1.1. Ceramic based solid composite electrolyte with Epoxy polymer infiltration-	19
3.1.2. Mechanical enhancement and thickness control of ceramic pellet	32
3.1.3. Electrochemical characterization	41
3.2. Patterned sintering oxide ceramic for the thin and flexible solid electrolyte.....	49
3.2.1. Ceramic sintered as specific pattern with sacrificial template	49
3.2.2. Mechanical properties of patterned ceramic based solid electrolyte	59
3.2.3. Electrochemical characterization	68
IV. Conclusion	75
V. References	77

List of Figures

Figure 1. Schematic image of Na-ion battery and material of each cathode, anode, and electrolyte parts. Copyright 2017, Chemical Society Reviews.^[22]

Figure 2. Concept image of all solid-state battery. Each of the cathode and anode parts contains solid electrolyte particles.

Figure 3. The trend of research results of composite electrolytes using oxide-based solid electrolytes to date. Copyright 2020, Advanced Science^[67]

Figure 4. Illustrative analysis of ion transfer characteristics according to the ratio of ceramics in a composite electrolyte using an oxide-based solid electrolyte. Copyright 2019, ACS Applied Energy Materials^[84]

Figure 5. Comparison data of ion transfer scheme and actual ion conductivity in ceramic-polymer composite electrolyte using NASICON solid electrolyte.

Figure 6. (a) Ionic conductivity measured by EIS analysis of NASICON powder. (b) Ionic conductivity measured by NASICON in sintered pellet state through EIS analysis.

Figure 7. Scheme image for Na ion transfer in powder and sintered states.

Figure 8. Schematic image of the entire experimental process of Epoxy-NASICON pellet synthesis.

Figure 9. (a) Cross-section SEM image of porous NASICON pellet and (b) EDS result data. (c) Cross-section SEM image of Epoxy-NASICON pellet and (d) EDS result data.

Figure 10. Porosity investigation result of NASICON pellet according to actual final sintering temperature.

Figure 11. (a) XRD result data of prepared NASICON powder and ICSD reference data peak. (b) XRD peak change of NASICON pellet according to the final sintering temperature.

Figure 12. (a) and (b) shows EDS mapping result for each element of porous NASICON pellet. (c) and

(d) shows same as Epoxy-NASICON pellet.

Figure 13. Ionic conductivity result through EIS measurement analysis of Porous NASICON pellets.

Figure 14. Ionic conductivity result through EIS measurement analysis of Epoxy-NASICON pellets.

Figure 15. Measurement principle and calculation formula of actual bending strength test.

Figure 16. Results of bending strength test for each sample of Bare NASICON pellet, Epoxy-NASICON pellet and Epoxy polymer.

Figure 17. Breaking load graph of NASICON pellet and Epoxy-NASICON pellet by calculation formula.

Figure 18. Graph of change in measured resistance value according to the thickness of the actual solid electrolyte pellet. The measurement area is equal to 0.50 cm^2 .

Figure 19. Comparison picture of the difference between the thicknesses of solid electrolytes that can be manufactured.

Figure 20. (a) Strength change scheme according to mixing of NASICON solid electrolyte and Epoxy polymer. (b) Changes in intensity are expected according to the rule of mixture.

Figure 21. TGA analysis result for each NASICON, Epoxy-NASICON and Epoxy polymer sample.

Figure 22. Measurement of electrochemical stability through CV analysis of Epoxy-NASICON sample.

Figure 23. Coin cell manufacturing scheme using solid electrolyte image.

Figure 24. (a) Charge/discharge performance of Na/Epoxy-NASICON/Na₃V₂(PO₄)₃ half-cell. Cell test performed at 0.1 C-rate and room-temperature. (b) Cycle performance data of Na/Epoxy-NASICON/Na₃V₂(PO₄)₃ half-cell.

Figure 25. Bipolar stacking scheme image using solid electrolyte pellet. Cell performed at 0.1C rate and room temperature and checked the coin cell of 7V class up to 10 cycles.

Figure 26. Suggest research directions for solid electrolytes in the future.

Figure 27. Various models of the rule of mixture and predicted values for lower bound calculation. It is possible to predict changes in physical properties of materials that are aligned.

Figure 28. Schematic image of patterned ceramic solid electrolyte sintering method using template

Figure 29. Actual appearance of each carbon template sample.

Figure 30. TGA/DSC result data of each carbon template sample from 25°C to 900°C.

Figure 31. Heating step of carbon templated NASICON ceramic.

Figure 32. Variation by temperature of the carbon template sample impregnated with the actual ceramic precursor solution.

Figure 33. Comparison of the actual shape of each carbon template and the shape of the ceramic remaining after the final sintering.

Figure 34. SEM image and thickness of a single strand of carbon fiber. SEM image of the ceramic solid electrolyte finally sintered using the carbon fiber.

Figure 35. Patterned ceramic sintered at a concentration of 0.3 M ceramic precursor. After the final sintering, it can be confirmed that the ceramic inner density is low.

Figure 36. Patterned ceramic sintered at a ceramic precursor concentration of 1 M. After the final sintering, it is possible to check the high internal density of the ceramic.

Figure 37. Cross-section SEM image of the final sintered NASICON ceramic using wizmac template. The sintering of ceramics capable of ion transfer in a zigzag shape.

Figure 38. Epoxy-NASICON SEM cross-section image with Epoxy polymer added to patterned sintered NASICON ceramics and EDS analysis results.

Figure 39. Cross-sectional SEM image of Epoxy-NASICON solid electrolyte. Ion transfer channel through ceramic can be checked.

Figure 40. Testing the bending properties using an acrylic cylinder. Experiments with cylinders 5 to 1 cm in diameter.

Figure 41. TGA analysis results of basic NASICON ceramic, epoxy polymer, and patterned sintered epoxy-NASICON samples.

Figure 42. Electrochemical stability analysis through LSV test of each sample.

Figure 43. The appearance of the patterned sintered epoxy-NASICON sample and the result of ion conductivity measurement through EIS analysis.

Figure 44. Measurement of ion conductivity through analysis of solid electrolyte and EIS by applying UV curing ETPTA polymer to patterned sintered NASICON.

Figure 45. Na / NVP half cell performance and cycle graph made using patterned sintered NASICON solid electrolyte.

List of Tables

Table 1. Summary of research results and characteristics of composite electrolytes using oxide-based solid electrolytes to date.

Table 2. Comparison of resistance according to the actual ionic conductivity and thickness ratio of commercialized liquid electrolyte and solid electrolyte pellets

Table 3. Measurement specification and result of actual bending strength for each solid electrolyte pellet sample

I. Introduction

1.1 Basic principle of Li ion and Na-ion battery system

In modern society, the importance of energy storage devices continues to be important. With the popularization of mobile devices, the expansion of use of electric vehicles (EVs), and the need for a large-scale energy storage system (ESSs), the demand for various energy storage devices is increasing. As the demand for eco-friendly energy increases, the demand for a large-scale energy storage system for storing electric power from unstable power generation systems such as solar energy, wind energy, and tidal energy is increasing. Research into rechargeable batteries that can meet this has been ongoing for a long time. Among them, among the battery systems that are commercially available and have great potential for future use, there is a Li-ion batteries (LIBs) system. LIBs with high energy and power densities have been commercialized since 1990s and have been applied to small portable devices.¹⁻⁴ The development of LiCoO_2 , a layered cathode material, and the initial LIBs system using graphite anodes have contributed greatly to commercialization of LIBs.⁵⁻⁷ Through continuous research and development, the current LIBs has an energy density of $250 \text{ Wkg}_{\text{cell}}^{-1}$, and is being developed to have a higher energy density and stability in order to use the LIBs system as an EVs and a ESSs in the future.

Lithium, the main element in LIBs, not evenly distributed on the earth. As a consequence the Andean states were called the 'new Middle-East'.⁸ However, the price of Li has skyrocketed due to the recent increase in demand for large-scale ESS and mobile devices and various energy storage devices. According to estimates, in 2008, worldwide Li consumption amounted to 21,280 tons, which is estimated to be consumed within 65 years by current resources,^{9, 10} rendering implementation of the above-mentioned applications difficult and very expensive. Sodium, by contrast, is the fourth largest element on the planet and is evenly distributed.¹¹ With abundant resources, much cheaper sodium carbonate can be produced, which is the driving force for SIB to replace LIB.^{12, 13} SIB is a sufficiently attractive system because of the recent demand to replace lithium in high-capacity energy systems.¹⁴ SIB started at the same time in the 1970s and 1980s, when the initial LIB was studied, but it fell behind in the field of research due to the rapid development and commercialization of LIB research.¹⁵⁻²⁰ Moreover, at that time, it was difficult to see the original performance of the battery because there were not enough facilities and materials to handle sodium. In the 1980s, a small number of US and Japanese companies produced SIB using sodium-lead alloy materials and P2-type Na_xCoO_2 materials. This SIB showed characteristics of more than 300 cycles in the initial stage, but at that time, it did not attract attention because it showed discharge contact voltage of 3.0V or less compared to the average voltage of the carbon / LiCoO_2 cell, 3.7 V.²¹

The battery components and the SIBs and LIB's electrical storage system are the same except for their ion carriers. Since the intercalation chemistry of sodium and lithium is very similar, similar compounds can be used for SIB and LIB, respectively. However, the biggest difference is that Na (1.02 Å) and

Li(0.76 Å) ions are different in size, which affects the mobility of the ions and the stability of the interface formation.⁹ In addition, sodium has a heavier weight than lithium(23 g mol⁻¹ compared to 6.9 g mol⁻¹) and has a high standard electrode potential(-2.71 V vs. SHE as compared to -3.02 V vs. SHE for lithium), which has disadvantages in terms of energy density. The weight of cyclable Li or Na is, however, a small fraction of the component mass, and the capacity is primarily determined by the characteristics of the host structures that serve as electrodes. Therefore, in principle, the transition from LIBs to SIBs should have no effect on energy density.¹² Furthermore, Li cannot be used as a current collector because it causes an alloy reaction with aluminum below 0.1 V vs. Li/Li⁺, but aluminum can be used for sodium cells. Therefore, SIB can replace the copper used in the cathode portion with aluminum, leading to price competitiveness.

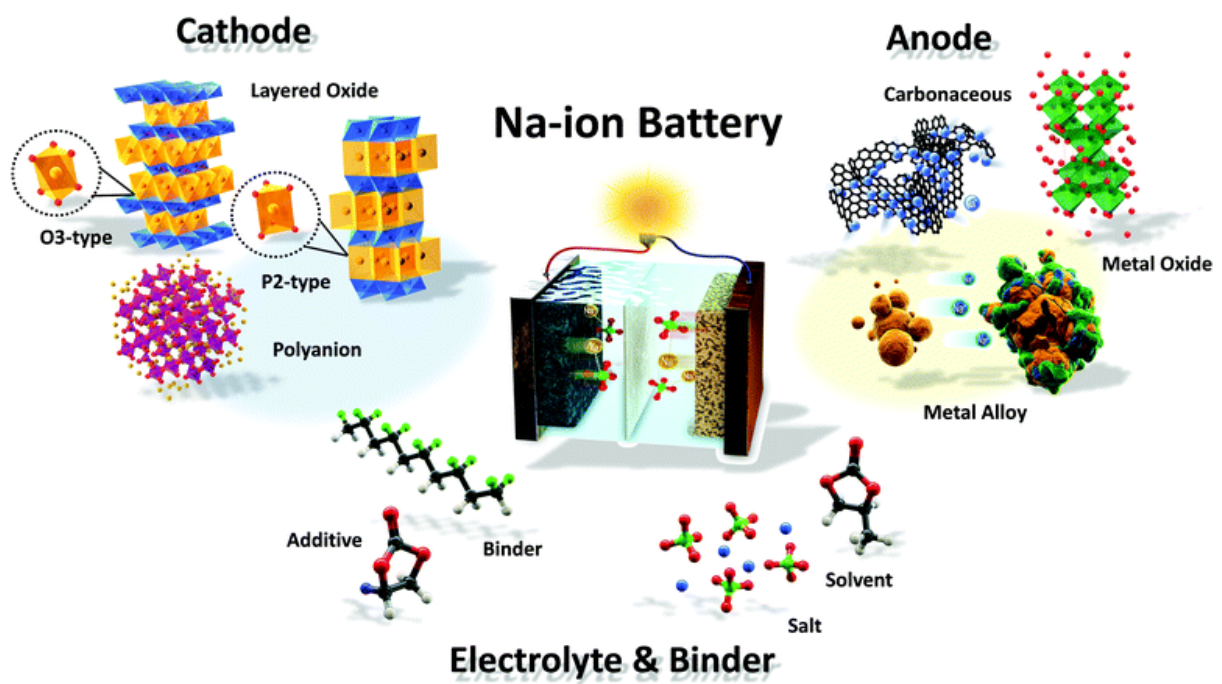


Figure 1. Schematic image of Na-ion battery and material of each cathode, anode, and electrolyte parts.
Copyright 2017, Chemical Society Reviews²²

1.2. Current safety issue of organic liquid electrolyte

The SIB system is basically like the LIB system. Even in the SIB system, the electrolyte uses an existing organic liquid electrolyte. The organic liquid electrolyte is used by dissolving Na salts such as NaPF₆, NaClO₄, and NaTFSI in organic solvents such as ethylene carbonate(EC), propylene carbonate(PC), dimethyl carbonate(DMC), and diethyleneglycol dimethylether(DEGDME). In electrolytes using these solvents, there is always a problem with thermal stability. Organic solvents can become fuel at the time of ignition and are particularly susceptible to high current, overcharge, overheating or damage to the battery. In addition, there is a phenomenon in which oxygen gas is emitted when reacting with a positive electrode material. As heat is produced faster than it can be dissipated, this condition is subject to thermal runaway, contributing to the cell bursting and combustion on air interaction with oxygen, and eventually to fire and explosion. The low viscosity organic solvents most widely found in LIBs or SIBs also have rather high vapor pressures, producing flame-retardant vapors upon elevated temperatures.²³ The problem of thermal safety of the organic liquid electrolyte is an issue that is always discussed in order to use the LIB and SIB system as an EVs or ESSs in the future. Specific techniques for addressing safety issues were examined for organic electrolyte, including the use of voltage of temperature-sensitive separators and overload security additives. Research on new electrolyte systems that are essentially non-flammable must be actively conducted.

1.3. All-solid-state battery system for Na-ion batteries

2.3.1 Solid electrolyte for all-solid-state batteries

From this point of view, it is ideal to use a new material to replace the existing liquid electrolyte in order to create an ultimately stable battery system and the solid electrolytes(SEs) material is the most representative material to replace the existing organic liquid electrolyte. All-solid-state batteries(ASSBs) employing nonflammable SEs have attracted great attention as promising alternative to conventional SIBs owing to their ultimate safety and potential to surpass the energy density of SIBs by stacking bipolar electrodes and minimizing inactive components in the battery pack.^{24, 25} The SEs are included in both the anode and cathode layers as well as the electrolyte layer, as shown in the figure image, to help ions move well throughout the cell. SEs are largely divided into a polymer electrolyte and an inorganic solid electrolyte. Most polymer electrolytes are mixed Li and Na salt with polymer chains such as polyethylene oxide(PEO) and polyacrylonitrile(PAN) and have been studied in a variety of ways because they are physically flexible and competitive in price. However, due to the nature of the polymer material, the ion conductivity is low at room temperature, and at a high temperature of 100 degrees or higher, the polymer material ignites making it difficult to use.²⁶ Electrochemical stability is also difficult to use above 4V, so it is necessary to compensate for the disadvantages.

The inorganic solid electrolyte is further divided into a sulfide-based solid electrolyte and an oxide-based solid electrolyte. The sulfide-based solid electrolyte has a high ionic conductivity comparable to that of a conventional liquid electrolyte, and thus was expected as a substitute material. In 2011, it was demonstrated that $\text{Li}_{10}\text{GeP}_2\text{S}_{12}$ (LGPS) has an ionic conductivity of $1.2 \times 10^{-2} \text{ Scm}^{-1}$.²⁷ In 2016, $\text{Li}_{9.54}\text{Si}_{1.74}\text{P}_{1.44}\text{S}_{11.7}\text{Cl}_{0.3}$ surpassed this mark with a $2.5 \times 10^{-2} \text{ Scm}^{-1}$ ionic conductivity and incorporation of the sulfide in an all solid-state battery.²⁸ After the first development of cubic Na_3PS_4 with a relatively high Na ion conductivity of over 10^{-4} Scm^{-1} in 2012²⁹, researches for developing new Na-ion-conductive sulfides have rapidly increased among the sodium ion-conducting solid electrolyte. In 2016, a good Na-ion conductivity of $1 \times 10^{-3} \text{ Scm}^{-1}$ was achieved in $\text{Na}_{2.9375}\text{PS}_{3.9375}\text{Cl}_{0.0625}$ ³⁰ with sodium vacancies and sodium antimony sulfide, Na_3SbS_4 ³¹⁻³³. Additionally, some other sulfides including $\text{Na}_{11}\text{Sn}_2\text{PS}_{12}$ ^{34, 35} and Na_3SbSe_4 ³⁶ shows ionic conductivity higher than 10^{-3} Scm^{-1} at 25 °C. Characterizing the mechanical stability of sulfide glasses and crystalline materials in LIBs and SIBs is critical in assessing their viability as solid electrolytes. Significant mechanical stresses develop in the solid electrolyte during the operation of a solid-state battery due to 1) Volume change of electrode material during charge / discharge and 2) Surface side reactions as the cycle progresses.^{37, 38} This results in poor interfacial contact cause local electrochemical polarization due to the structural heterogeneity of the electrode material and poor electrochemical efficiency. Having a relatively low elastic modulus can reduce interfacial resistance by simply cold pressing. In the battery system using the existing liquid electrolyte, the liquid can penetrate sufficiently into the pores inside the electrode, but the solid-state battery needs an additional method to sufficiently contact the electrode and the electrolyte. Anode and cathode active materials are usually ball-milled with conductive additive and sulfide solid electrolyte, respectively, to ensure enough electronic and ionic conductivity in the composites before to pressing into electrode pellets. The sulfide-based solid electrolyte basically has a “soft” characteristic, and thus, it exhibits good contact with only physical pressing. The remaining disadvantages of sulfide-based solid electrolytes are low electrochemical stability and instability to moisture. The low electrochemical stability of sulfide-based solid electrolytes has also been reported experimentally, especially when it encounters lithium metal or high voltage positive electrode materials. In addition, it reacts with moisture in the air to hydrolysis and emit toxic gas, H_2S , which must be handled in an inert gas atmosphere and makes it difficult to use in normal situations.³⁹

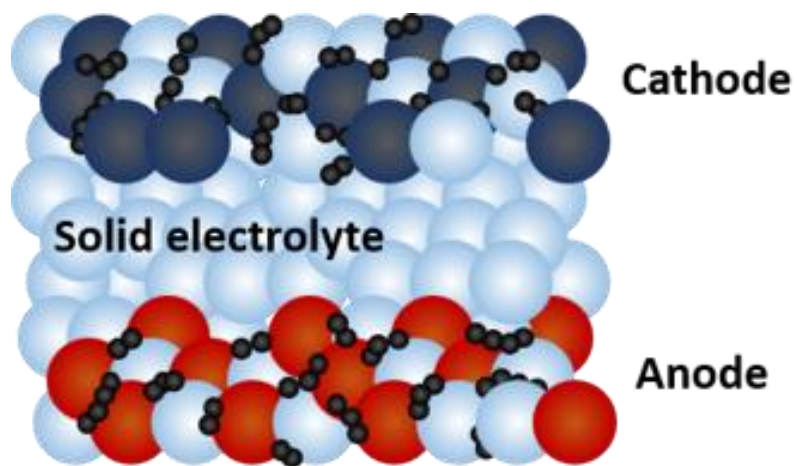


Figure 2. Concept image of all solid-state battery. Each of the cathode and anode parts contains solid electrolyte particles.

2.3.2 Properties of Oxide ceramic solid electrolytes

In contrast to sulfide-based solid electrolytes, oxide-based solid electrolytes have highly stable electrochemical, thermal, and chemical properties.⁴⁰ In practice, the oxide-based solid electrolyte is stable in air and electrochemically does not decompose to more than 7V, and is a ceramic material that is stable up to 1000 degrees. Among the oxide-based solid electrolytes in the early model, LiPON is stable solid electrolyte to Li metal⁴¹, and it is a promising candidate for ASSBs due to its electrochemical stability.⁴² However, the ionic conductivity of LiPON is around 10^{-6} S cm⁻¹ and this conductivity is very low compared to the liquid electrolyte used in conventional lithium ion batteries. The oxide-based solid electrolytes containing Ti, such as $\text{Li}_{3-x}\text{La}_{(2/3)-x}\text{TiO}_3$ (LLTO) and $\text{Li}_{1.3}\text{Al}_{0.3}\text{Ti}_{1.7}(\text{PO}_4)_3$ (LATP), show high Li⁺ ion conductivity.^{43,44} Researchers have suggested that trivalent cations such as Al³⁺, Sc³⁺, Ga³⁺, Fe³⁺, In³⁺ and Cr³⁺ replacing partial Ti⁴⁺ cations in $\text{Li}_{1+x}\text{R}_x\text{Ti}_{2-x}(\text{PO}_4)_3$ can increase conductivity where $\text{Li}_{1.3}\text{Al}_{0.3}\text{Ti}_{1.7}(\text{PO}_4)_3$ (LATP) can increase ionic conductivity by 7×10^{-4} S cm⁻¹. In addition, the ion radius of M⁴⁺ cations will affect the $\text{LiM}_2(\text{PO}_4)_3$ (M = Ge, Hf, or Zr) lattice constants as well to further affect to the tunnel size through which Li⁺ can pass.⁴⁵ And $\text{Li}_7\text{La}_3\text{Zr}_2\text{O}_{12}$ (LLZO) is one of the new materials by *Weppner et al.* This has ionic conductivity of 10^{-3} S cm⁻¹ and is not react by Li metal anode^{46,47}. LLZO has a crystal garnet structure and has 3-dimensional Li⁺ ion conduction way. Among the sodium ion conductive oxide-based solid electrolytes, historically β -Alumina electrolyte is the first fast ion conductor used in industrial Na-S and Na-metal chloride batteries.^{48,49} β -alumina single crystal is stated to have an unusually high ionic conductivity of 1 S/cm at 300 °C, 4 times higher than that of its polycrystalline phase (0.22–0.35 S/cm at 300 °C, but only 2.0×10^{-3} S/cm at room temperature).⁵⁰ NASICON (NA Super Ion CONductor) is one of the most popular oxide-based solid electrolytes, and has a 3D structure suitable for Na ion transfer, which goes beyond β -Alumina electrolyte. The solid covalent structure of NASICON is of considerable functional value and demonstrates good thermal and chemical stability.⁵¹⁻⁵³ Goodenough and Hong reported a solid solution between $\text{NaZr}_2\text{P}_3\text{O}_{12}$ and $\text{Na}_4\text{Zr}_2\text{Si}_3\text{O}_{12}$ as the first NASICON compound ($\text{Na}_{1+x}\text{Zr}_2\text{Si}_x\text{P}_{3-x}\text{O}_{12}$ ($0 \leq x \leq 3$), abbreviated as NZSP).^{54,55} The word NASICON refers to a substance with the following crystal structure with a general composition formula of $\text{AMP}_3\text{O}_{12}$, where the A site can be occupied by monovalent cations (e.g. Li⁺, Na⁺, K⁺), divalent cations (e.g. Mg²⁺, Ca²⁺, Ba²⁺, Cu²⁺, Co²⁺), trivalent cations (e.g. Al³⁺, Y³⁺) and tetravalent cations (e.g. Ge⁴⁺; Zr⁴⁺; Hf⁴⁺); and the M sites can be occupied by divalent cations (e.g. Cd²⁺, Mn²⁺, Co²⁺, Ni²⁺, Zn²⁺), trivalent cations (e.g. Al³⁺, Ga³⁺, Y³⁺), tetravalent cations (e.g. Ti⁴⁺; Si⁴⁺; Zr⁴⁺) and pentavalent cations (e.g. V⁵⁺; Nb⁵⁺; Sb⁵⁺).⁵⁶ For NASICON-type $\text{Na}_3\text{Zr}_2\text{Si}_2\text{PO}_{12}$ compound, the ionic conductivity shows 6.7×10^{-4} S/cm at room temperature and 0.2 S/cm at 300 °C.^{54,55} The ionic conductivity at room temperature up to 10^{-3} S/cm was observed in the doped-NZSP and NHSP conductors.^{57,58}

As such, the oxide-based solid electrolyte material itself exhibits high ionic conductivity but is difficult to use due to its high grain boundary resistance.^{43, 59} As the grain boundary became the biggest problem in ion transfer, it became a major obstacle to the production of a solid state battery using an oxide-based solid electrolyte. The sulfide-based solid electrolyte was able to transfer ions by simply applying pressure due to its relatively soft properties.⁶⁰ Grain boundary resistance is often marginal⁶¹ and can only be detected when the conductivity exceeds $10^{-2} \text{ S cm}^{-1}$ to have a very low impedance response from bulk.⁶² However, in case of a powder state oxide-based solid electrolyte, no matter how high the pressure is applied to create contact between particles, the interfacial resistance cannot be reduced as much as a sulfide-based material. Interfacial resistance between solid particle is not important for connecting the particles in solid electrolyte based on sulfide, while high grain boundary resistance is a critical problem in oxide-based systems. As a result, although the oxide-based solid electrolyte has an ion conductivity of 10 or more, it is difficult to make a bulk-type solid-state battery. An oxide-based solid electrolyte which is exceptionally used in solid-state batteries of bulk-type is an oxide-based material despite having an ionic conductivity as low as $10^{-6} \text{ S cm}^{-1}$. As described above, since the polymer solid electrolyte, sulfide-based solid electrolyte, and oxide-based solid electrolyte have distinct advantages and disadvantages, research and development are continuously conducted in each field.

2.3.3 Current research trend of Oxide ceramic solid electrolyte

Our research group has continued to conduct research and development to replace liquid electrolytes by utilizing oxide-based solid electrolytes. As mentioned earlier, the oxide-based solid electrolyte is a very stable material, but due to the brittle nature of the material itself, it has difficulty in application in commercial battery system due to its high grain boundary resistance. Various methods have been devised to solve this interfacial resistance problem, but the current research trend is not only to use one substance of an oxide-based solid electrolyte, but also to mix and use a liquid electrolyte or a polymer electrolyte with an oxide-based solid electrolyte. This mixed solid electrolyte is called a solid composite electrolytes(SCEs), and various solid electrolyte materials, polymer materials, and liquid electrolytes are mixed to find optimal conditions.⁶³⁻⁷⁰ In general, liquid or polymer electrolyte materials have more flexible properties than oxide-based solid electrolytes, so when used together, it was expected that interface resistance of existing oxide-based solid electrolytes could be reduced due to sufficient contact with the surface of solid electrolytes. The ionic conductivity is mainly determined by the transfer mechanism. In the oxide-based solid electrolyte itself,^{71, 72} ion transport can move rapidly through vacancies or interstitial ions, but in the polymer matrix, ions move while repeating breaks/formation conditions through an electric field.⁷³⁻⁷⁵ In the early model of the composite electrolyte, the proportion of the oxide-based solid electrolyte was mixed only by about 10 ~ 20wt% to see the effect of the ceramic filler. The ceramic process functions as plasticizer, which decrease the crystallinity of polymers and

enhances the amorphous shape and thus boosts the mobility of Li ions.^{76, 77} Additionally, the acidic groups on the ceramic surface have high affinity with anions, which tends to dissociate lithium salts, contributing to enhanced free Li ion concentration.⁷⁸⁻⁸⁰ However, since polymer electrolyte's inherent low ionic conductivity restricts the great enhancement of the overall ionic conductivity of SCEs. The ionic conductivity of SCEs is therefore not appropriate for functional use in all-solid-state batteries at room temperature. The ionic conductivity of SCEs recorded in previous work is summarized in Figure 3. It could be found that the ionic conductivity of most as-prepared samples in temperatures varying from 20 to 40 °C is lower than 10^{-4} S cm⁻¹, while that of other samples could exceed the order of 10^{-4} S cm⁻¹.

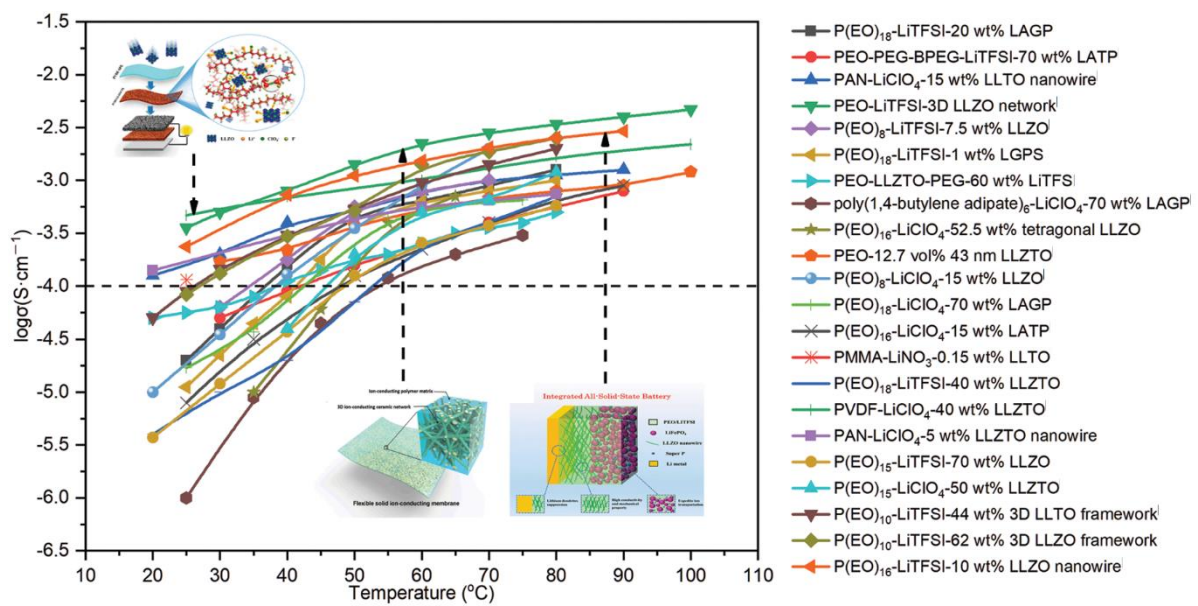


Figure 3. The trend of research results of composite electrolytes using oxide-based solid electrolytes to date. Copyright 2020, Advanced Science⁶⁷

To overcome this, there have been studies to highlight the advantages of oxide-based solid electrolytes by reducing the proportion of polymer electrolytes and increasing the proportion of ceramics in SCEs. It was expected that the oxide-based solid electrolyte would not only stop with the effect of a ceramic filler, but rather, ions would pass through the ceramic solid electrolyte. Tracking the path of movement of Li or Na in the SCE is important to increase the ion transport mechanism and design the SCE structure in the future.⁸¹ The ion transport pathway of SCE is largely composed of a polymer phase, a ceramic phase, and an interface between polymer and ceramic. Identifying the regulated pathway during ion migration is still not obvious. Hu and co-workers⁸² tracked lithium ion transport pathways in 50wt% LLZO-P(EO)₁₈/LiClO₄ electrolyte using selective isotope labeling and high-resolution solid-state Li NMR. In the LLZO-P(EO)₁₈/LiTFSI method, Zheng and Hu⁸³ have examined the impact of ceramic solid electrolyte concentration on Li ion transport pathways. It is observed that the principal ion transfer pathway changes from polymer to ceramic phase with the change in the fraction of the LLZO group. Li NMR was seen to move through Li NMR, but the problem is that the ionic conductivity is too low when it is passed through ceramic phase. As mentioned earlier, it is difficult to transfer ions due to large interfacial resistance with only the oxide-based solid electrolyte powder. This shows the same problem as the proportion of ceramics in SCEs increases. When the ionic conductivity was measured while gradually increasing the proportion of the ceramic solid electrolyte in the SCEs through actual experiments, it was confirmed that as the proportion of the ceramic increased, the ionic conductivity gradually decreased, especially when it was 50wt% or more, there was a sharp drop in ion conductivity. In the Figure 4, there are experiments on actual Li ion conducting SCEs using LLZO solid electrolyte.⁸⁴ The results of the Na ion conducting SCEs experiment using NASICON solid electrolyte can be also confirmed by experiment in Figure 5. Similar experimental results can be confirmed for both Li and Na ceramics. Both results show a decrease in ion conductivity as the proportion of the ceramic solid electrolyte increases.

SE film	Conductivity (S/cm)	Thickness (μm)	Component ratio (Ceramic : Polymer)	Thermal stability	Ref
PEO-PVP/ NaF salt	1.1×10^{-7} (RT)	N/A	15wt% : 85wt%	N/A	<i>Physica B.</i> 2011 , 1706-1712
EP-PEG/ SiO ₂ Nanopowder	1.0×10^{-6} (RT)	N/A	10wt% : 90wt%	N/A	<i>J. Materials Chemistry A.</i> 2013 , 1, 8348
PEO-NaTFSI/ SiO ₂ Nanopowder	1.0×10^{-5} (40°C)	~200	10wt% : 90wt%	< 150°C	<i>J. Power Sources.</i> 2014 , 248, 695-702
PEO-NaClO ₄ / TiO ₂ Nanopowder	2.6×10^{-4} (60°C)	180-200	5wt% : 95wt%	N/A	<i>J. Power Sources.</i> 2015 , 278, 375
PEO-NaFSI/ NASICON powder	4.4×10^{-5} (RT)	200-400	40wt% : 60wt%	< 150°C	<i>J. Mater. Chem. A.</i> 2016 , 4, 15823-15828
PEO-NaTFSI/ Na _{3.4} Zr _{1.8} Mg _{0.2} Si ₂ PO ₁₂	6.0×10^{-5} (30°C)	200-300	50wt% : 50wt%	< 237°C	<i>J. Power Sources.</i> 2017 , 372, 270-275
PEO-NaClO ₄ / SiO ₂ powder	1.6×10^{-4} (60°C)	N/A	5wt% : 95wt%	N/A	<i>Materials Letters.</i> 2019 , 236, 13-15
PEO-NaClO ₄ / Na ₃ Zr ₂ Si ₂ PO ₁₂ powder	2.1×10^{-5} (RT)	~100	25wt% : 75wt%	N/A	<i>ACS Materials. Lett.</i> 2019 , 1, 1, 132-138

Table 1. Summary of research results and characteristics of composite electrolytes using oxide-based solid electrolytes to date.

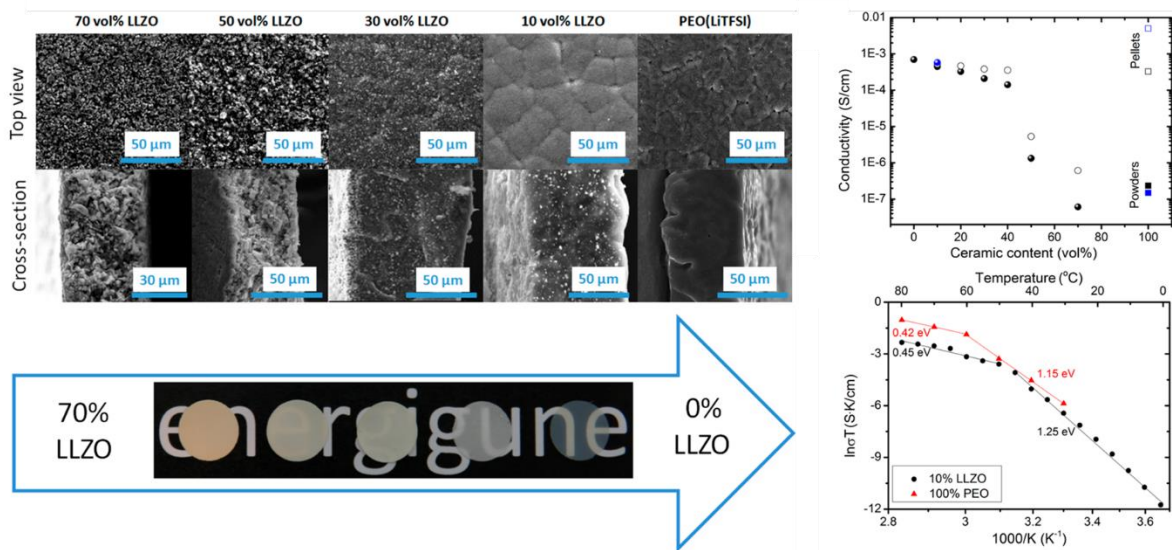


Figure 4. Illustrative analysis of ion transfer characteristics according to the ratio of ceramics in a composite electrolyte using an oxide-based solid electrolyte. Copyright 2019, ACS Applied Energy Materials⁸⁴

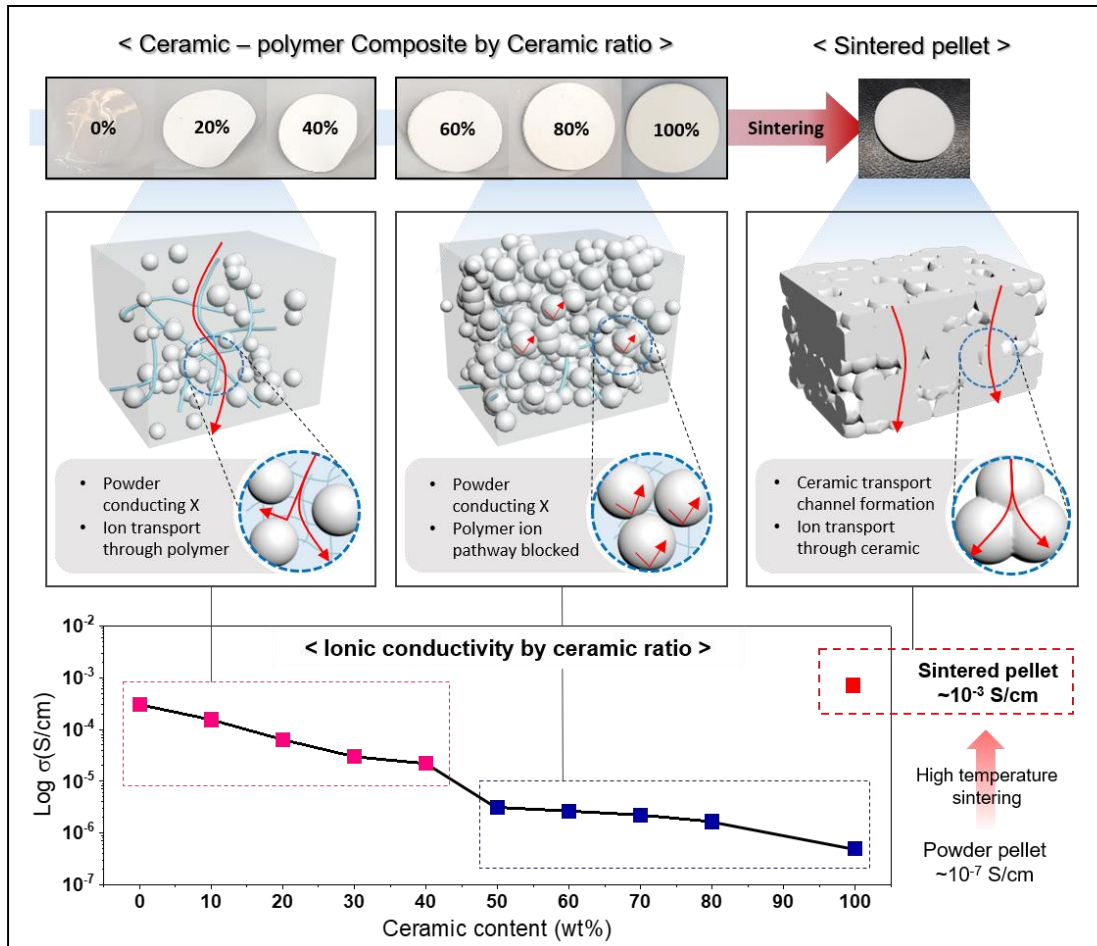


Figure 5. Comparison data of ion transfer scheme and actual ion conductivity in ceramic-polymer composite electrolyte using NASICON solid electrolyte.

As a result, the combination of the oxide-based solid electrolyte powder and the polymer electrolyte has a limitation in increasing the ratio of the oxide-based solid electrolyte. Thus, to see the ion transfer effect through the oxide-based solid electrolyte, it is necessary to remove the interface resistance through sintering in the conventional manner. However, this also must solve the problems of brittle characteristics and thick form, which are disadvantages of the oxide-based solid electrolyte after sintering. Accordingly, recently, a method of sintering a ceramic solid electrolyte to secure an ion transfer channel of a ceramic first, and then compounding it with a polymer electrolyte material to have physical properties in a film form has been studied. Yang co-workers^{85, 86} reported an ice-templating method to fabricate PEO-based composite electrolyte with vertically aligned and connected LATP nanoparticles. As such, the recent SCE issue is progressing toward sintering the oxide-based solid electrolyte in a form optimized for ion transport, forming a solid electrolyte ion transport channel, and then proceeding with polymer complexation. So far, most of the research has been conducted in the field of Li-ion batteries, so many studies have not been made in the field of Na-ion batteries. In the field of Na-ion batteries, SCEs research are still stuck on how to mix ceramic powder and polymer electrolyte. As motivated by issues, in this study, a composite electrolyte in a Na ion battery using an oxide-based solid electrolyte was conducted. To confirm the possibility of ion conduction of ceramic solid electrolyte, a method of intentionally sintering a ceramic solid electrolyte with a high porosity and filling internal pores with a polymer material to increase physical strength was used. In this way, the physical properties can be expected to increase in strength due to the use of polymer materials, while the ion conduction effect can be transferred through the sintered solid ceramic to create a high stability solid ceramic electrolyte. As the oxide-based solid electrolyte, $\text{Na}_3\text{Zr}_2\text{Si}_2\text{PO}_{12}$ (NASICON) solid electrolyte was used, and epoxy-NASICON solid electrolyte pellets were prepared by filling the internal pores with Epoxy-resin polymer material⁸⁷, and the possibility of using the electrolyte in Na-ion battery was confirmed. As such, it is expected that the composite of polymers and ceramics may have strengths exceeding the limits of conventional oxide solid electrolytes and may be made into thin electrolytes having thinner films.

Moreover, sintered to have a specific pattern of Na ionic solid electrolyte, it has a faster ionic conductivity and has a higher physical strength and flexibility. To sinter the ceramic in a specific pattern, the NASICON precursor solution was made into a complete solution, impregnated with a template of a specific shape, and then the template was sintered. In this way, the physical properties can be enhanced by combining the polymer material with the sintered ceramic in a specific shape. The resulting patterned sintered SCEs have an ionic conductivity of 10^{-4} Scm^{-1} and have flexible properties under $200\mu\text{m}$ thickness. Cell characteristics were also confirmed using $\text{Na}_3\text{V}_2(\text{PO}_4)_3$ cathode and Na metal, and cell characteristics of 7V class or higher were also confirmed through bipolar stacking to confirm the possibility of utilization as a solid electrolyte.

II. Experimental

2.1. Preparation of materials

To synthesis of $\text{Na}_3\text{Zr}_2\text{Si}_2\text{PO}_{12}$ NASICON powder, using a solid state reaction with a stoichiometric mixture of sodium phosphate dodecahydrate ($\text{Na}_2\text{PO}_4 \cdot 12\text{H}_2\text{O}$, Sigma), silicon dioxide (SiO_2 , Sigma), zirconium dioxide (ZrO_2 , Sigma). The mixture of precursors was ball-milled, subjected to 1st calcination at 400°C for 5 hours, and then 2nd calcination at 1050°C for 12 hours. After that, intermediate ball-milling, then sintered at 1190°C for 10 hours. The resultant NASICON powder was ground well, affording an average particle size of 2~3 μm . For the sintered pellet, pressed NASICON powder at 300Mpa pressured die. The powder is cold pressed to form pellets and then sintered. First, sintering at 400°C for 4 hours, 800 degrees for 4 hours, and then at 1100°C for 10 hours. By controlling the final sintering temperature, the porosity of the pellets can be controlled. Although the NASICON crystal phase appears at a 1000°C-sintering temperature, the pores are too large without sintering, and the sintering is completed from 1100°C or higher to secure the ceramic ion transfer passage. Finally, from 1260°C or more, the pores are reduced to less than 1% and sintered to a perfect crystal state.

The NASICON solution used to make a template was prepared as follows. Each precursor was prepared as sodium hydroxide (NaOH , Sigma), Zirconium(IV) propoxide ($\text{Zr}(\text{OC}_3\text{H}_7)_4$, 70wt% solution in 1-propanol, Sigma), Tetraethyl orthosilicate ($\text{Si}(\text{OC}_2\text{H}_5)_4$, Sigma), trimethyl phosphate ($(\text{CH}_3\text{O})_3\text{PO}$, Sigma). Each precursor is dissolved in ethanol according to stoichiometry. In the case of the existing water-soluble precursor solution, a white condensate remains when all precursors are mixed. The NASICON powder was made using the condensate, but all precursors were completely dissolved in the ethanol-based solution.

To synthesis of $\text{Na}_3\text{V}_2(\text{PO}_4)_3$ (NVP) cathode material, vanadium(V) oxide (V_2O_5 , Sigma), sodium phosphate monobasic (NaH_2PO_4 , Sigma), oxalic acid dihydrate ($\text{C}_2\text{H}_2\text{O}_4 \cdot 2\text{H}_2\text{O}$, Sigma) were purchased from Sigma-Aldrich. All materials were used as received. Here V_2O_5 , $\text{C}_2\text{H}_2\text{O}_4 \cdot 2\text{H}_2\text{O}$, NaH_2PO_4 were stoichiometric mixed at ethanol by planetary ball-mill in a grinding jar at 300 rpm for 15 h. The mixture turned from yellow to light green at the end of the process, indicating the completion of the reduction V^{5+} to V^{3+} by oxalic acid. After evaporating away, the ethanol, a uniform green fine powder was obtained. $\text{Na}_3\text{V}_2(\text{PO}_4)_3$ was synthesized by decomposing the above powder at 350 °C in N_2 for 5 h. After a thorough grinding operation, the powder was pressed into a tablet and sintered at 750 °C for another 10 h in N_2 to obtain $\text{Na}_3\text{V}_2(\text{PO}_4)_3$.

Epoxy-resin polymer was prepared as follows. Monomer bis (4-glycidyaloxyphenyl) propane and 1,3-phenylenediamine are dissolved in Tetrahydrofuran (THF) at 1M and stirred for 1 hour to dissolve completely. Each solution is then mixed at a volume ratio of 2 : 1 and stirred again for 1 hour. The mixed solution is used as an epoxy-resin polymer solution.

The ionic liquid electrolyte is prepared by mixing sodium trifluoromethanesulfonic (NaTFSI, sigma-Aldrich) salt and 1-Butyl-1-methylpyrrolidinium bis(trifluoromethylsulfonyl)imide (Py₁₄TFSI, sigma-Aldrich) ionic liquid at 1M concentration.

2.2. Preparation of solid electrolytes and electrodes

After impregnating the pore NASICON pellet in the epoxy-resin solution, it is maintained in a vacuum to be absorbed to the internal pores. After repeating the above three times, the NASICON sample absorbing the epoxy polymer is heat-treated at 150 degrees for 24 hours. After checking the sample, a brown epoxy-NASICON sample can be obtained.

As the cathode active material for the cell test, Na₃V₂(PO₄)₃(NVP) material was used. The cathode slurry mixes an NVP active material, a super-P conductive agent, an ionic liquid electrolyte, and a Polyvinylidene fluoride (PVDF) binder at a weight ratio of 70: 10: 10: 10.

In the anode part, UV curing polymer electrolyte layer is made between Na metal and solid electrolyte. The UV curing polymer electrolyte prepared by mixing Trimethylolpropane ethoxylate triacrylate (ETPTA, sigma-Aldrich), NaTFSI and Triethylene glycol dimethyl ether (TEGDME, Daejung) at a weight ratio of 45:15:40. Then, drop and mix 2-hydroxy-2-methylpropiophenone as an initiator before use. The mixed solution is dropped on the surface of the solid electrolyte, and then covered with a release film made of Polypropylene (PP) and cured by irradiating UV (365 nm) for 15 minutes.

Afterwards, Na metal was placed on the surface of the UV curing polymer electrolyte, and a cell test in which a Na metal/solid electrolyte/cathode was made was placed in a 2032 coin cell. All steps were processed in a glove box with less than 10 ppm of both oxygen and moisture. When manufacturing a bipolar stacked cell, a coin cell was prepared by putting Al foil between the two solid electrolyte cells as described above.

2.3. Characterization

The NASICON solid electrolyte material characterization has been investigated through X-ray diffraction (XRD) studies using a Bruker D8 Advance X-ray diffractometer with a Cu K α X-ray source and the measurements were recorded with a 2θ range of 10-80°. Scanning electron microscope (SEM) image and Energy dispersive spectrometer (EDS) of the films were taken on Verios 460, FEI and XFlash 6130, Bruker operated at accelerating voltage of 10KV.

Thermogravimetric analysis was performed by adjusting the rate of temperature increase as 1 °C/min from room temperature to 700 degrees in an air atmosphere. The instrument used was a Q500 model from TA instruments.

The bending strength test was calculated by KS L 1591 three-point strength measurement and was

measured by the Korea Institute of Ceramic Technology at a measuring speed of 0.5mm / min.

The bending strength test was calculated by KS L 1591 three-point strength measurement, and was measured by the Korea Institute of Ceramic Technology at a measuring speed of 0.5mm / min.

Electrochemical impedance spectroscopy (EIS) measurements were performed by Pt sputtering both sides of solid electrolyte pellets and electrochemical characterization using SUS electrodes. Bio-logic VSP-300 models were electrochemically tested at a frequency range of 7 MHz to 100 MHz and 10 mV. Ionic conductivity calculates followed equation.

$$\sigma = \frac{l}{A} \times \frac{1}{R}$$

where σ is ionic conductivity(S/cm), l is thickness of sample(cm), A is measuring area(cm) and R is total resistance(Ohm, Ω).

III. Results and Discussion

3.1. Epoxy-NASICON solid electrolyte pellet after sintering process

3.1.1. Ceramic based composite electrolyte with Epoxy polymerization

Basically, the oxide-based solid electrolyte material has a hard and brittle property. Since the powder has the same properties, it is difficult to form a perfect contact between powders, even at high pressures. Due to these problems, it is difficult to expect normal ion conduction when measuring ionic conductivity in powder state. As shown in Figure 6(a), the ionic conductivity of 10^{-7} S / cm is measured when the powder oxide solid electrolyte pressed at high pressure state about 300Mpa. The NASICON powder sample was fine grinded as under $1\mu\text{m}$ particle size and isotactic press in alumina mold state at dry room. This means that no matter how even the solid electrolyte powder is packed evenly, Na ions do not pass between the powder and the powder and thus do not exhibit normal ionic conductivity. For this reason, when the cell assembled using solid electrolyte powder, normal cell operation is difficult due to poor ion transfer. Here, the most basic way to reduce the resistance between the powders is to sinter at high temperature. When the same sample is subjected to a high temperature sintering process as it is, the surface of the solid electrolyte powder melts to each other and the interfacial resistance between the solid electrolytes is minimized. Therefore, at Figure 6(b), the ionic conductivity of the same sample after sintering is measured to be 7.8×10^{-4} S / cm. The expected Na ion transport scheme for each state is shown in Figure 7. Through this, a high temperature sintering process is essential for using an oxide-based solid electrolyte.

However, as mentioned above, sintering an oxide-based solid electrolyte still has a hard and brittle characteristic. Therefore, although it has high ionic conductivity, it is difficult to manufacture a physically thin film form, so it is not easy to apply practical use at commercial battery system. As can be seen from the table in Table 2, the overall conductivity of the solid electrolyte is lower than that of the liquid electrolyte, but the actual Na ion conductivity is similar. In the case of the solid electrolyte, unlike the liquid electrolyte, since the anion does not move, only Na ions move. This can be confirmed by Na ion transference number, which is 0.2 ~ 0.3 for most liquid electrolytes, but solid electrolyte has 1 transference number. For this reason, solid electrolytes can be sufficiently used in terms of ionic conductivity. However, when the actual usable thickness is compared with the separator thickness of the existing liquid electrolyte, the actual thickness of the solid electrolyte pellet is at least 30 times thicker than that of commercial separators. Because of this difference in actual use thickness, the actual resistance value is bound to be greatly different. Therefore, if the oxide-based solid electrolyte can be manufactured in a higher strength and used in a thin form, it will be enough to replace the organic liquid electrolyte.

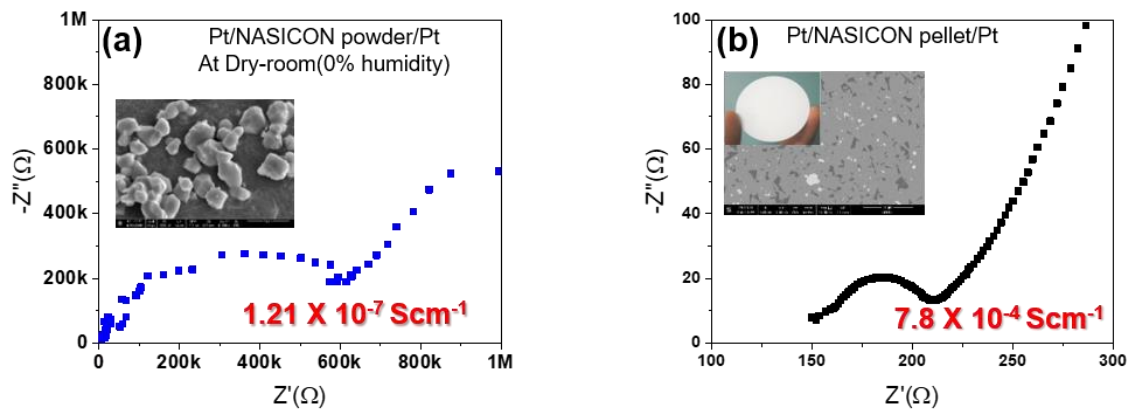


Figure 6. (a) Ionic conductivity measured by EIS analysis of NASICON powder. (b) Ionic conductivity measured by NASICON in sintered pellet state through EIS analysis

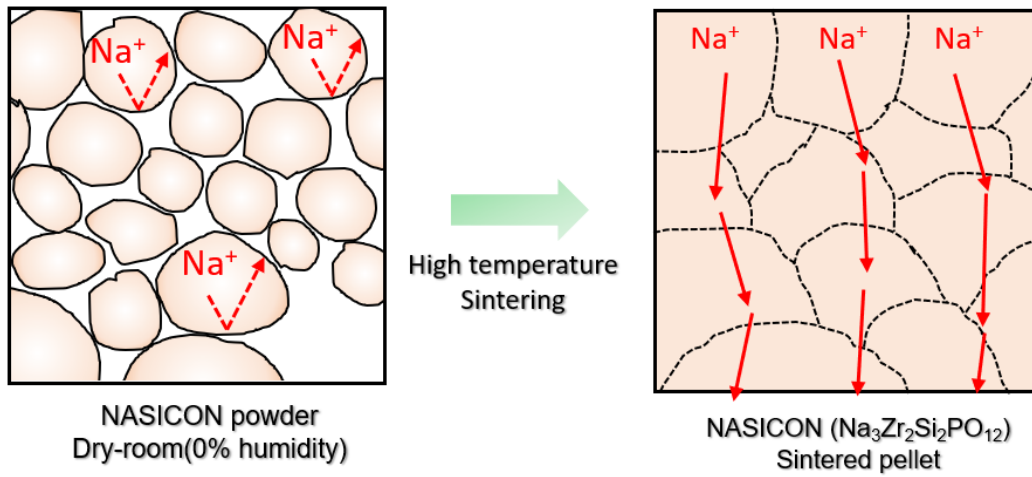


Figure 7. Scheme image for Na ion transfer in powder and sintered states.

<i>*Salt concentration : 1M</i>	Total conductivity(S/cm)	Na⁺ ion conductivity(S/cm)	Thickness(μm)	Total resistance(Ω) (calculated)
NaPF ₆ /PC	8.0 x 10 ⁻³	5.8 x 10 ⁻³	~ 25	~ 0.21
NaClO ₄ /PC	6.4 x 10 ⁻³	5.6 x 10 ⁻³	~ 25	~ 0.22
NaCF ₃ SO ₃ /TEGDME	1.0 x 10 ⁻³	5.0 x 10 ⁻⁴	~ 25	~ 2.49
NaTDL/PC	4.0 x 10 ⁻³	6.0 x 10 ⁻⁴	~ 25	~ 1.03
NaPF ₆ /EC	6.8 x 10 ⁻³	2.0 x 10 ⁻³	~ 25	~ 0.62
NaClO ₄ /DMC	5.0 x 10 ⁻³	1.0 x 10 ⁻³	~ 25	~ 1.24
NaTFSI/EC,DMC	3.7 x 10 ⁻³	7.4 x 10 ⁻⁴	~ 25	~ 1.68
NASICON	7.8 x 10 ⁻⁴	7.8 x 10 ⁻⁴	~ 900	~ 230

Table 2. Comparison of resistance according to the actual ionic conductivity and thickness ratio of commercialized liquid electrolyte and solid electrolyte pellets

In order to increase the strength of the ceramic pellets, a denser pellet manufacturing method has been used through a change in the manufacturing process.⁸⁸⁻⁹⁰ Higher density of pellets and fewer pores result in relatively higher strength. But ultimately, the strength of the material nature is limited, so there is a limit to reducing the thickness to actual use. Therefore, we have been able to increase the physical strength by incorporating polymer materials of different strengths in addition to ceramic materials. Figure 8 shows a scheme image for the sintering of ceramics and the process of composite polymeric materials into the sintered ceramics. Conventional solid ceramic electrolytes in powder form have made it difficult for Na ions to pass along the ceramic, no matter how physically pressured it is. Even when the ion conductivity was measured in a state in which a ceramic powder was put in a mold and a pressure of 300Mpa or more was applied, only about 10^{-7} S/cm ionic conductivity appeared. After all, the physical pressure alone cannot exceed the interfacial resistance between the ceramic powders, and it is necessary to eliminate the interfacial resistance through the sintering process. When a ceramic sample subjected to pressure is sintered for 10 hours at over 1000 °C in a heat treatment furnace, the surface of the ceramic powder melts and a channel for Na ions pathway is created. The final sintering temperature is adjusted to intentionally increase the porosity of ceramic pellet. The pores thus prepared can be polymerized after filling the polymer material in the monomer state. Impregnating ceramic pellets in a liquid state monomer to maintain a vacuum state can sufficiently fill the polymer material into the pores of the ceramic. In this experiment, Epoxy-resin polymer was used to increase the physical strength. Epoxy-resin is not an ion-conducting polymer material, so it is polished to reveal the surface of the solid electrolyte after polymerization. The result is a ceramic-polymer composite electrolyte as shown in the photo.

Figure 9 shows the SEM image of the sintered porous NASICON and Epoxy-NASICON after polymerization. After ceramic sintering, the NASICON crystals are completely physically attached, forming ion transport channels. Na⁺ ions can migrate through the ceramic solid electrolyte through the formed ion transport channels, as shown in the Figure 9(a). By controlling the final temperature, there is a difference in porosity of the ceramic, which can be confirmed by Figure 10. The crystal phase of NASICON ceramics starts to appear from 900 degrees, and sintering starts with the ceramic powder. XRD data confirms the appearance of NASICON crystals phase at Figure 11. From 900°C after NASICON crystal phase appears, the higher the temperature, the greater the crystallinity and the lower the internal porosity. The experimentally confirmed part is not fully sintered up to 900°C, so that NASICON powders do not stick together, but after 1000°C, ceramic crystals stick to each other and form a length to move ions. From 1200°C or more, there was almost no internal porosity, so we could not use the method we wanted to use. Finally, we used sintered ceramic at 1100°C. NASICON ceramics sintered at 1100°C show porosity of about 10%. Figure 10 shows how to calculate the porosity of each NASICON pellets. When the epoxy polymer is added to the sample, the polymer material is sufficiently

filled in the internal pores as shown in the Figure 9(c). In the SEM image, it was confirmed that the empty space between NASICON crystals was filled with a black material. The epoxy polymer seemed to be filled, and it was identified as a polymer material containing C through EDS analysis Figure 9(b) and (d). The detailed EDS analysis results for each component can be seen through the Figure 12. If you compare the components of Na, Si, Zr, P, which are contained in NASICON, and the C components that are only contained in Epoxy polymers by color, you can see that the Epoxy polymer is definitely contained in the inner pores. In the same sample, Na ions only move through the connected ceramics, so adding epoxy polymers does not affect about ion conducting. As a result of measuring ion conductivity through electrochemical impedance spectroscopy, NASICON ceramics sintered at 1100 degrees showed $1.76 \times 10^{-4} \text{ S cm}^{-1}$ (Figure 13) and $1.45 \times 10^{-4} \text{ S cm}^{-1}$ (Figure 14) after epoxy polymer treatment. The total resistance is also displayed within the error range, so the ionic conductivity values seem to be mostly maintained.

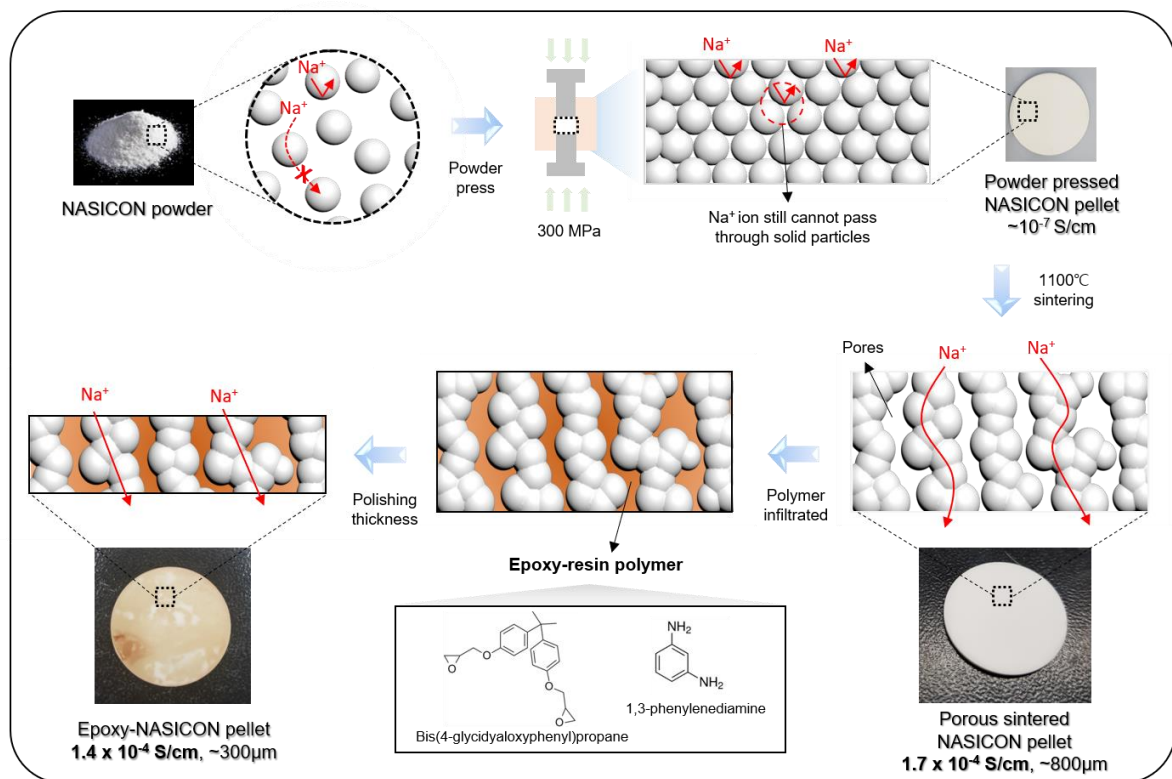
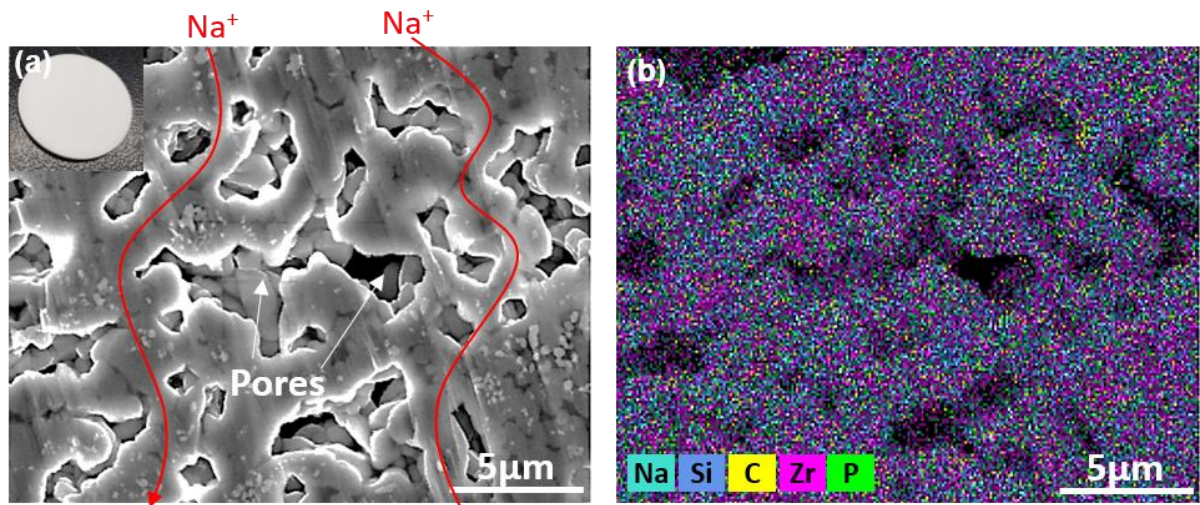
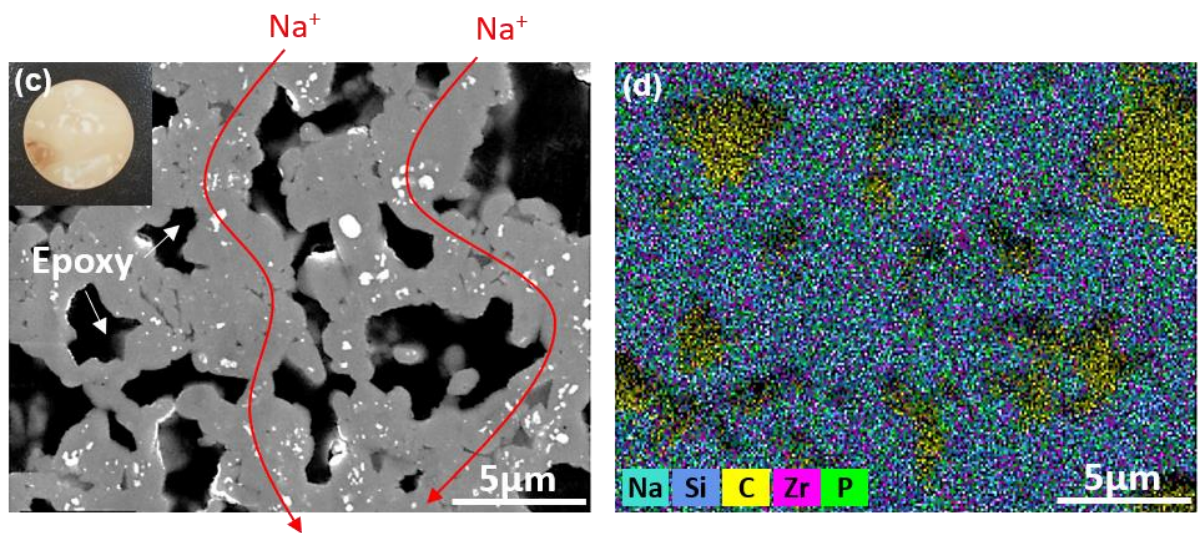


Figure 8. Schematic image of the entire experimental process of Epoxy-NASICON pellet synthesis.



< Porous NASICON cross-section >



< Epoxy - NASICON cross-section >

Figure 9. (a) Cross-section SEM image of porous NASICON pellet and (b) EDS result data. (c) Cross-section SEM image of Epoxy-NASICON pellet and (d) EDS result data.

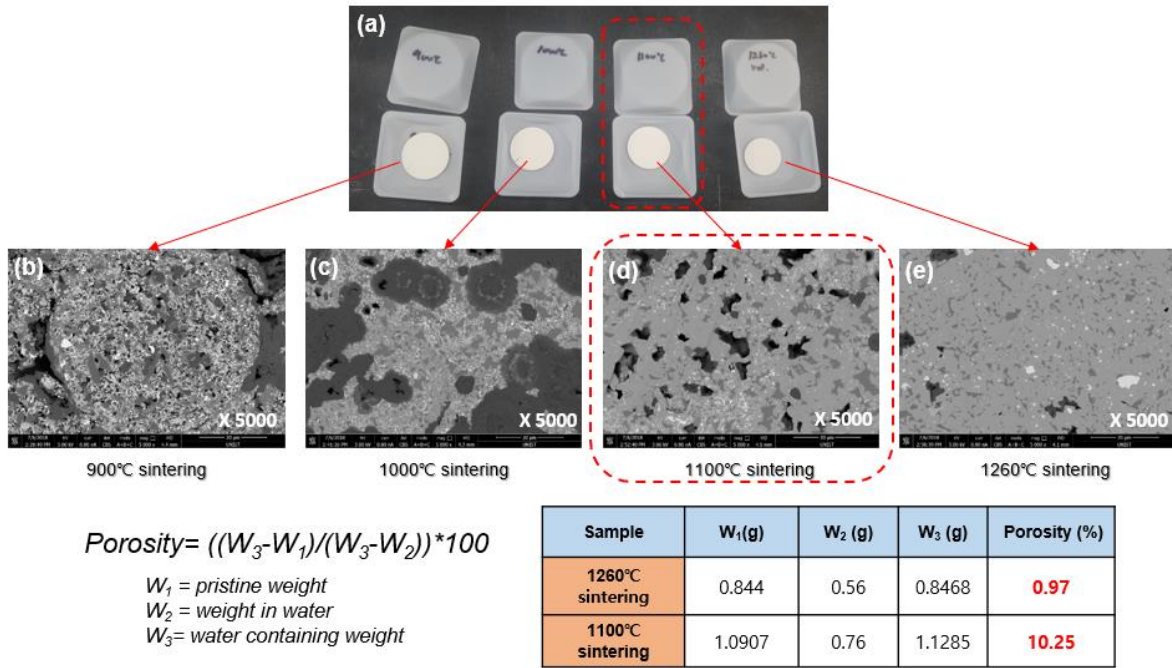


Figure 10. Porosity investigations result of NASICON pellet according to actual final sintering temperature

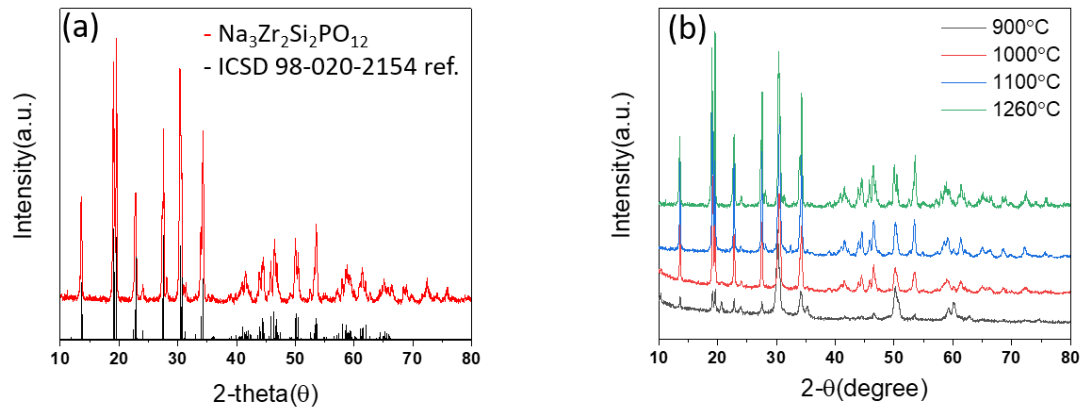


Figure 11. (a) XRD result data of prepared NASICON powder and ICSD reference data peak. (b) XRD peak change of NASICON pellet according to the final sintering temperature.

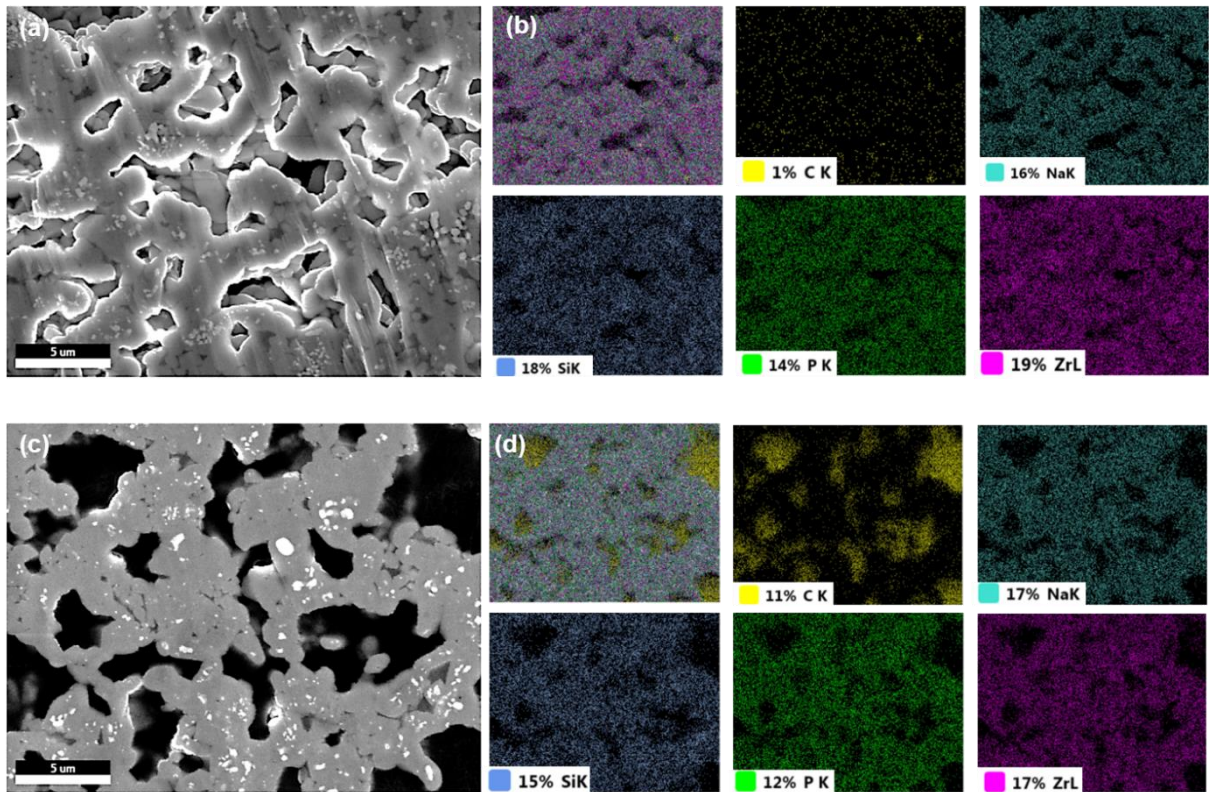


Figure 12. (a) and (b) shows EDS mapping result for each element of porous NASICON pellet. (c) and (d) shows same as Epoxy-NASICON pellet.

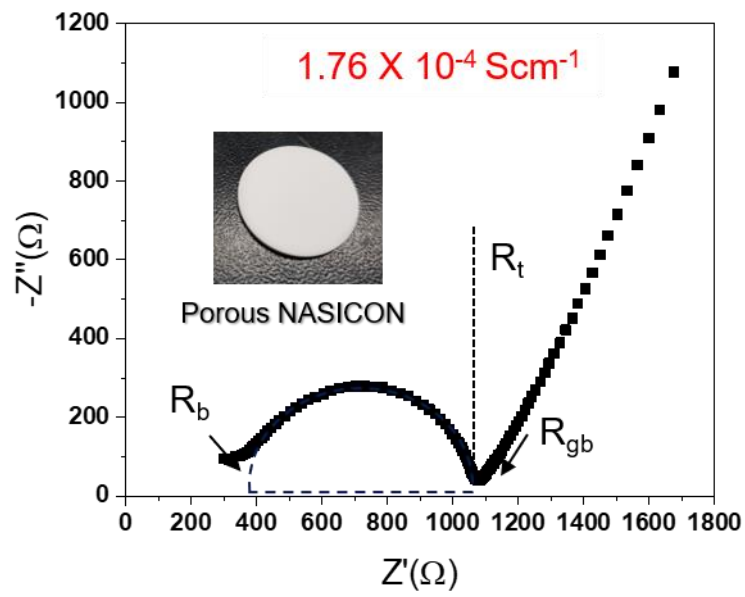


Figure 13. Ionic conductivity result through EIS measurement analysis of Porous NASICON pellets.

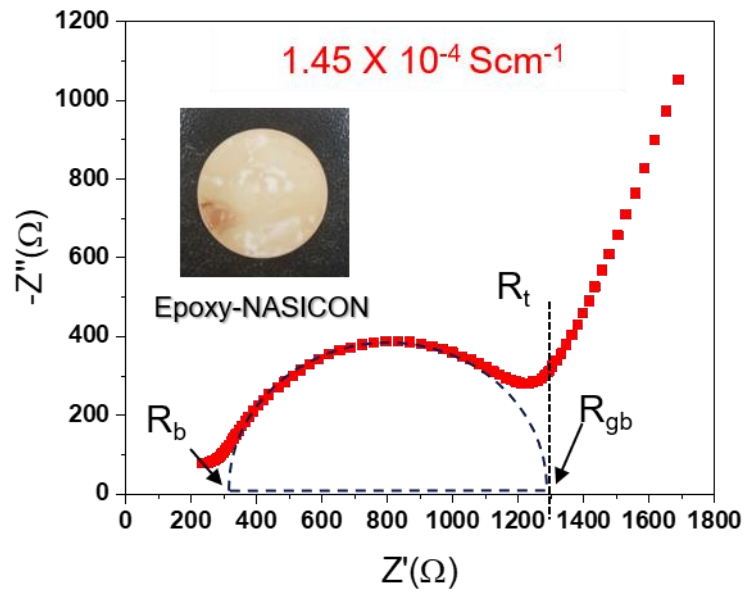


Figure 14. Ionic conductivity result through EIS measurement analysis of Epoxy-NASICON pellets.

3.1.2. Mechanical enhancement and thickness control of ceramic pellet

The strength test of the solid electrolyte was conducted by a flexural strength test. Flexural strength, also known as bending strength, is a method of measuring the force at break by applying a force to a specific specimen. The flexural strength represents the highest stress experienced within the material at its moment of yield. It is measured in terms of stress, here given the symbol σ . The scheme image and calculation formula for the experiment can be confirmed through the Figure 15. In this way, physical strength measurements of NASICON pellet solid electrolyte and NASICON solid electrolyte treated with epoxy polymer were performed.

The physical strength of the ceramic samples increased significantly after the epoxy polymer treatment. As shown in Figure 16, basically, NASICON ceramics have an average bending strength of 15Mpa even if they are sintered at higher density. Curing only epoxy polymer has an average bending strength of 150Mpa. Since the internal pores of the ceramic are not closed pores, curing occurs with the epoxy polymers connected to each other. This can be supported to prevent the ceramic from breaking inside, the epoxy-NASICON sample after the epoxy treatment can be seen that the average bending strength increases to 35Mpa. Experimental measurements of each substance can be found in Table 3. If the current measured bending strength value is calculated as the force that can withstand the actual use size, it is calculated as Figure 17. When we make the cell in our experiment, it takes about 0.8kgf of force to make sure that the solid electrolyte was broken after the coin cell is made. When bare NASICON pellets were used, they were mostly available in thicknesses of 800 μ m to 900 μ m. Epoxy-NASICON can be used for calculations with a thickness of less than 600 μ m and in a real experiment, a 500 μ m thick sample could be used. It is expected to be used more in the future because it can be used in a thinner state than the existing solid electrolyte with the same physical properties. Based on this, the thickness of epoxy-NASICON is reduced and the actual resistance is measured. Figure 18 shows that the resistance decreases in proportion to the thickness. Drawing a trendline based on the actual measured values results in a minimum thickness of 120 μ m to ensure that the solid electrolyte resists less than 100 Ω . If you look at the actual solid electrolyte sample through Figure 19, you can see that the existing 800 ~ 900 thickness NASICON sample can be reduced up to 300 thickness. If a solid electrolyte of a small thickness with the same strength and resistance value can be used, the applicability will increase in the future. The enhancement of physical property of epoxy-NASICON composite can be predicted by the rule of mixture formula that can be used to calculate the properties of a mixture of different physical properties.⁹¹ In Figure 20 shows actual strength with the calculated value of the rule of mixture. The maximum value that can be predicted by a general formula can be obtained by the following formula.

$$E_{composite} = fE_{epoxy} + (1 - f)E_{NASICON}$$

Where f is the volume fraction of the epoxy polymer, E_{epoxy} is the physical property (bending

strength) of the epoxy polymer, $E_{NASICON}$ is the physical property (bending strength) of NASICON ceramics, and $E_{composite}$ is the physical property of the epoxy-NASICON composite sample.

Also, the minimum predictable value can be obtained by the following formula.

$$E_{composite} = \left(\frac{f}{E_{epoxy}} + \frac{1-f}{E_{NASICON}} \right)^{-1}$$

The above expected values can be estimated from the maximum and minimum values according to the direction of the force applied to the material and can be estimated from the case where there are no internal pores of the composite material and the seamless connection with each other. In the case of the current epoxy-NASICON sample, as shown in Figure 20(a), the ceramic electrolyte is sintered, and the ceramics are seamlessly connected to each other. The inside of this ceramic is filled with epoxy polymer material without any remaining pores and polymerized without breaks, which appears to be the actual value close to the expected maximum value.

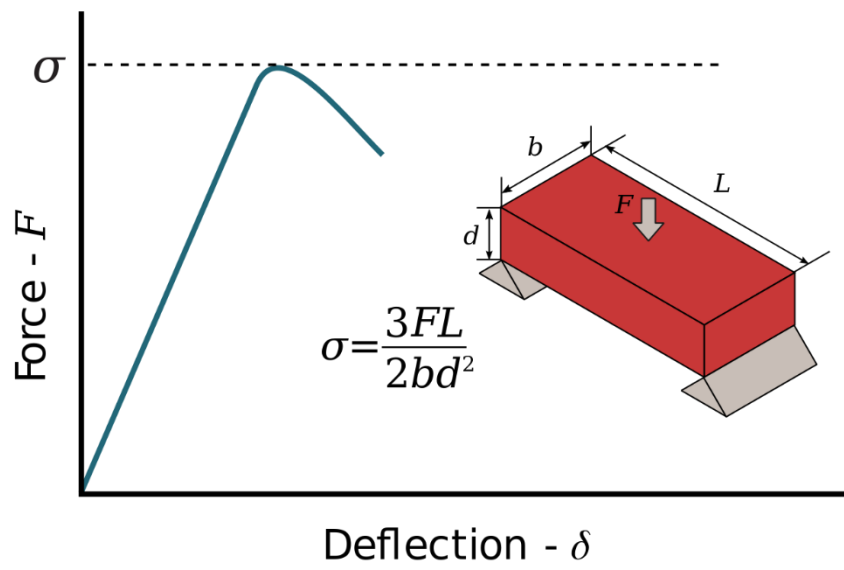


Figure 15. Measurement principle and calculation formula of actual bending strength test

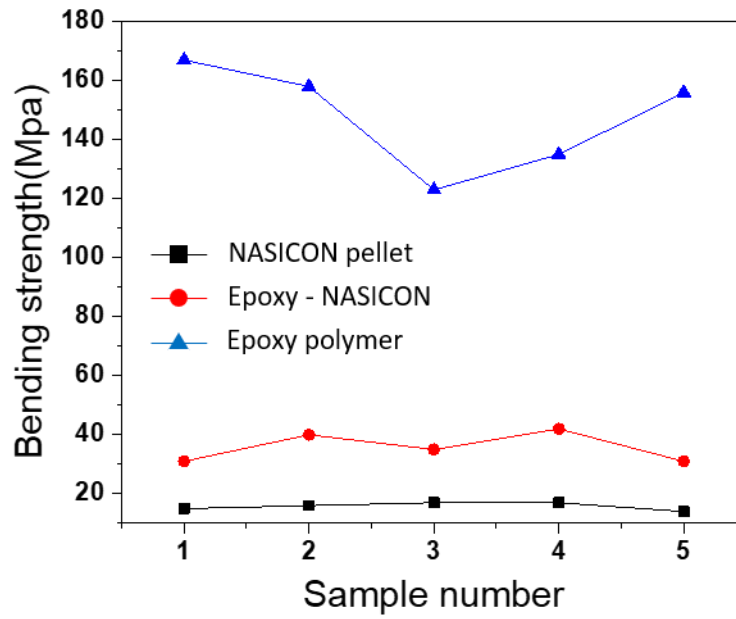


Figure 16. Results of bending strength test for each sample of Bare NASICON pellet, Epoxy-NASICON pellet and Epoxy polymer

	Sample number	Width(mm)	Thickness(mm)	Breaking load(kgf)	Bending strength(MPa)
NASICON ceramic	1	20.86	1.34	1.953	15
	2	20.86	1.34	2.087	16
	3	20.84	1.33	2.134	17
	4	20.88	1.34	2.123	17
	5	20.84	1.34	1.751	14
Epoxy-NASICON	1	20.83	1.30	3.704	31
	2	20.86	1.30	4.816	40
	3	20.94	1.31	4.331	35
	4	20.84	1.27	4.817	42
	5	20.93	1.32	3.885	31

Table 3. Measurement specification and result of actual bending strength for each solid electrolyte pellet sample

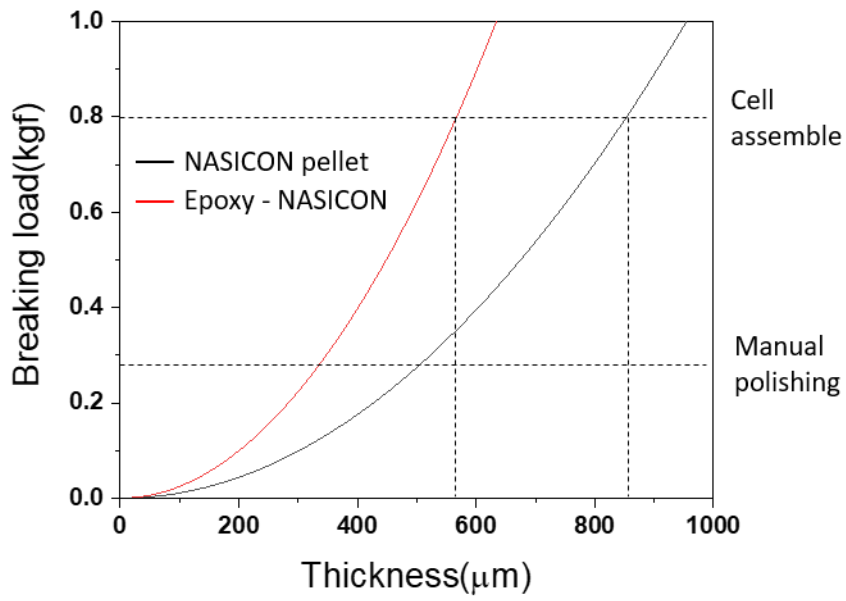


Figure 17. Breaking load graph of NASICON pellet and Epoxy-NASICON pellet by calculation formula.

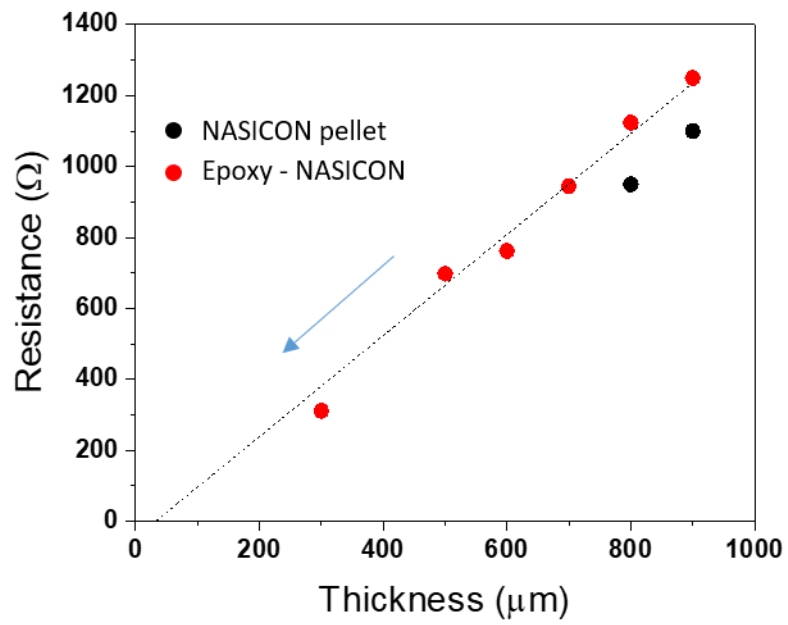


Figure 18. Graph of change in measured resistance value according to the thickness of the actual solid electrolyte pellet. The measurement area is equal to 0.50 cm².

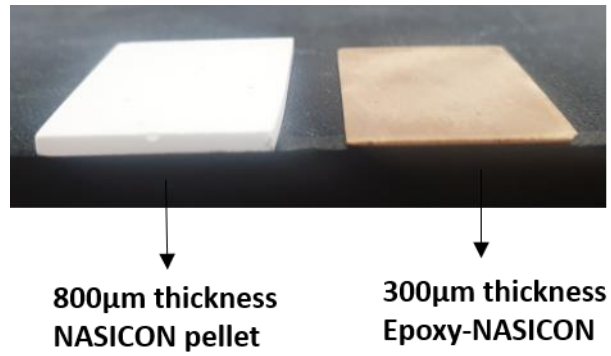


Figure 19. Comparison picture of the difference between the thicknesses of solid electrolytes that can be manufactured.

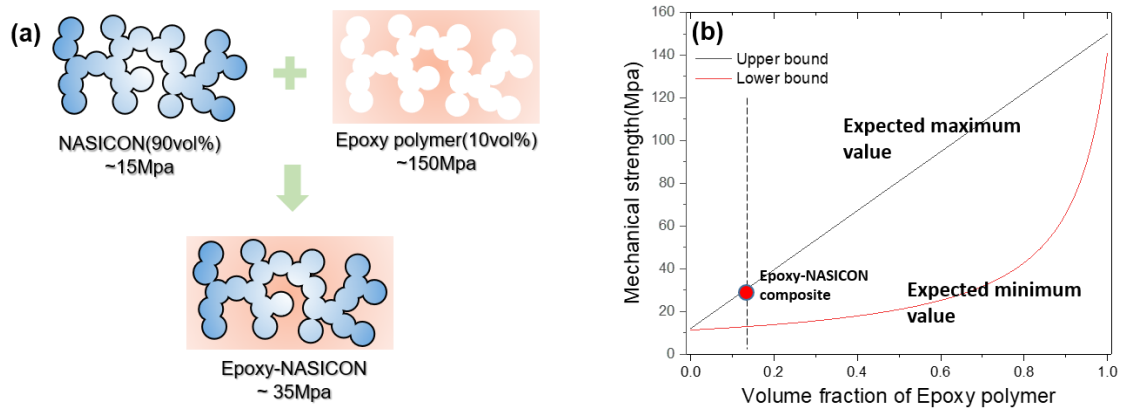


Figure 20. (a) Strength change scheme according to mixing of NASICON solid electrolyte and Epoxy polymer. (b) Changes in intensity are expected according to the rule of mixture.

3.1.3. Electrochemical characterization

Basically, NASICON ceramics are stable up to 700°C or more and epoxy polymers are stable up to 400°C after curing. This can be seen from the Thermogravimetric analysis(TGA) experiment in Figure 21. Since each material is stable above 400°C, the epoxy-NASICON sample mixed with the two materials is stable until 400°C. Cyclic voltammetry(CV) was conducted to confirm the electrochemical stability. In Figure 22, the result of epoxy-NASICON with Na metal showed no side reaction up to 7V except for plating/stripping of Na metal near 0V. It is believed that both NASICON ceramic and epoxy polymers are electrochemically stable and there are no other chemical reactions in the composite process.

To confirm the possibility of using an epoxy-NASICON electrolyte for a solid-state battery, a cell test was also carried out by attaching a positive electrode and a negative electrode, respectively. In fact, all-solid-state battery cell fabrication has not established an all-solid cell system that can show perfect cell performances. Since the positive electrode and the negative electrode material are currently used as a solid active material, the use of an electrolyte as a solid material causes a problem of contact resistance again. In addition, it is difficult to confirm the good cycle performance because the solid electrolyte is difficult to compensate for the volume change of the active material generated during charging and discharging. In this experiment, the cell design was carried out as follows to confirm the only for the applicability of epoxy-NASICON as a solid electrolyte. The cathode part was made by mixing a 10wt% of ionic liquid electrolyte within total cathode part in order to reducing interfacial resistance between cathode active material and solid electrolyte, and the anode part, Na metal, added UV curing polymer electrolyte layer between the solid electrolyte and the Na metal to minimize contact resistance. Since there is no liquid electrolyte leaked by the above process, ions move through the channel of the solid electrolyte during the charge and discharge process. The coin cell fabrication scheme using Epoxy-NASICON solid electrolyte is shown in Figure 23. As described above, when the half-cell of $\text{Na}_3\text{V}_2(\text{PO}_4)_3$ cathode material and Na metal was manufactured and charged and discharged at 0.1 C-rate, the capacity of about 120mAh/g and 20 cycles were stably driven. The charge and discharge graph can be seen in Figure 24. In addition, if the solid electrolyte is used, there is no leakage of the liquid electrolyte, so that a bipolar stack can be made in a single cell to produce a high voltage single cell. The bipolar stacked coin cell experiment result can be seen at Figure 25. In this experiment, a 7V class coin cell was fabricated by stacking two or more solid electrolyte cells in single coin cell. Through this, it is possible to confirm cell driving possibility by sufficiently ion-transferring role with epoxy-NASICON composite electrolyte.

So far, the strength and effect of NASICON solid electrolytes have been confirmed through epoxy polymer complexation. For the manufacture of thin and strong solid electrolytes, high-strength polymers such as epoxy were mixed in the pores of ceramics, and the possibility of increasing the

strength while maintaining the electrochemical properties was confirmed. However, current methods still have brittle characteristics, and there is a limit to making the thickness below 20 μm , which is the thickness of the conventional NIBs system. In addition, the presently used epoxy polymer material does not have an ion conduction effect, so the higher the ratio, the more difficult to expect the ion conductivity. In order to solve the above problems, additional research and development is required and presenting way the future aspect about oxide based solid electrolyte at Figure 26. As mentioned at the beginning of the paper, the sintering process is essential to secure ion transfer paths using ceramic solid electrolytes. Currently, the sintering process causes NASICON powders to stick randomly and appear only as a solid pellet. Therefore, further research is needed to sinter the ceramic electrolyte, but to have a specific pattern to secure the most efficient ion transfer channel and to have physical flexibility. In addition, Epoxy polymer material used to increase the strength is expected to have a higher ionic conductivity than if using a polymer electrolyte material having an ion conducting effect. If the above method is used, it is possible to manufacture a thin film solid electrolyte and to apply it to more fields.

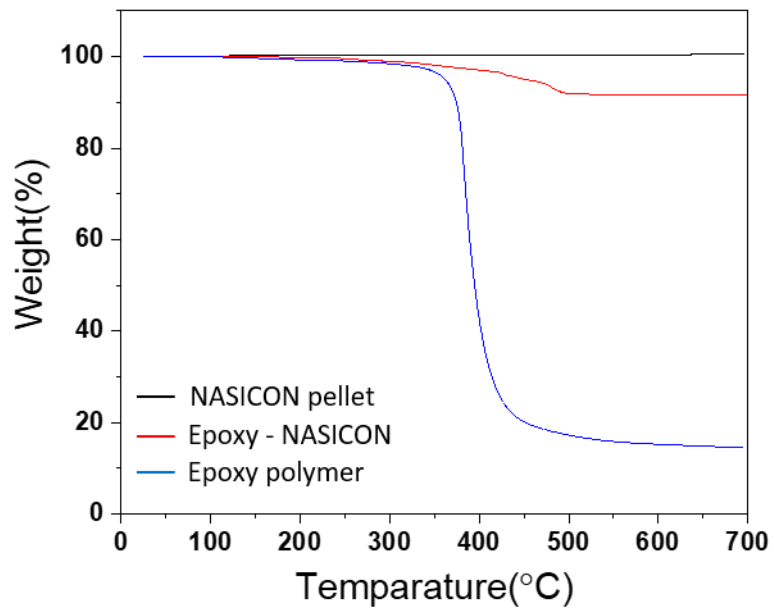


Figure 21. TGA analysis result for each NASICON, Epoxy-NASICON and Epoxy polymer sample.

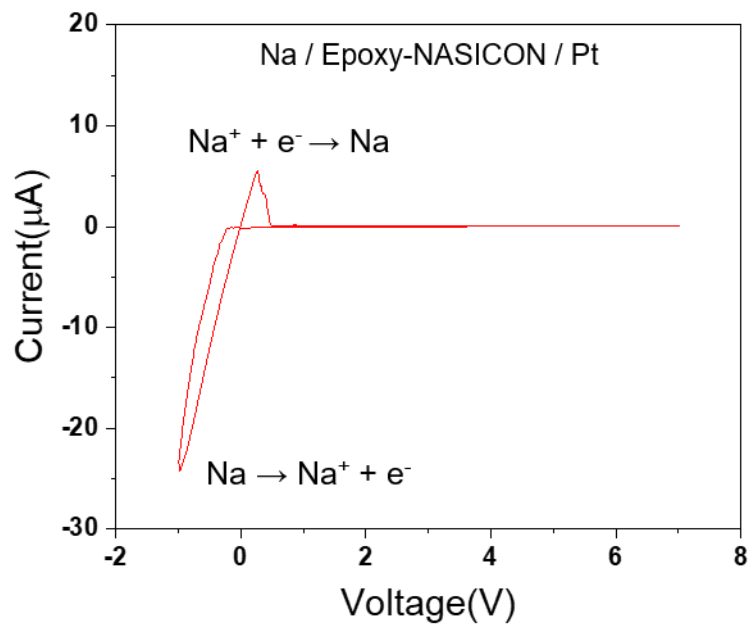


Figure 22. Measurement of electrochemical stability through CV analysis of Epoxy-NASICON sample.

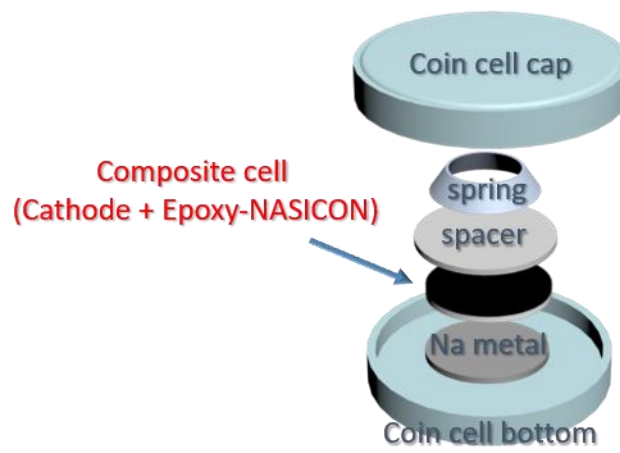


Figure 23. Coin cell manufacturing scheme using solid electrolyte image.

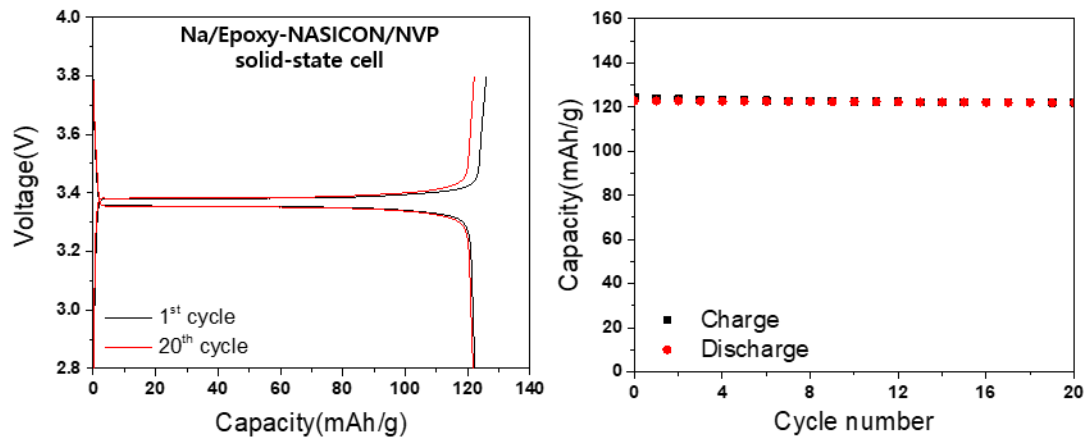


Figure 24. (a) Charge/discharge performance of Na/Epoxy-NASICON/ $\text{Na}_3\text{V}_2(\text{PO}_4)_3$ half-cell. Cell test performed at 0.1 C-rate and room-temperature. (b) Cycle performance data of Na/Epoxy-NASICON/ $\text{Na}_3\text{V}_2(\text{PO}_4)_3$ half-cell.

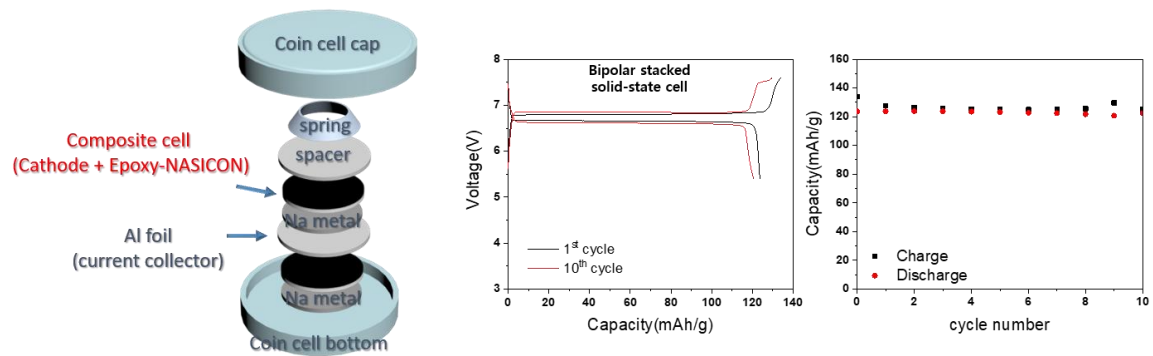


Figure 25. Bipolar stacking scheme image using solid electrolyte pellet. Cell performed at 0.1C rate and room temperature and checked the coin cell of 7V class up to 10 cycles.

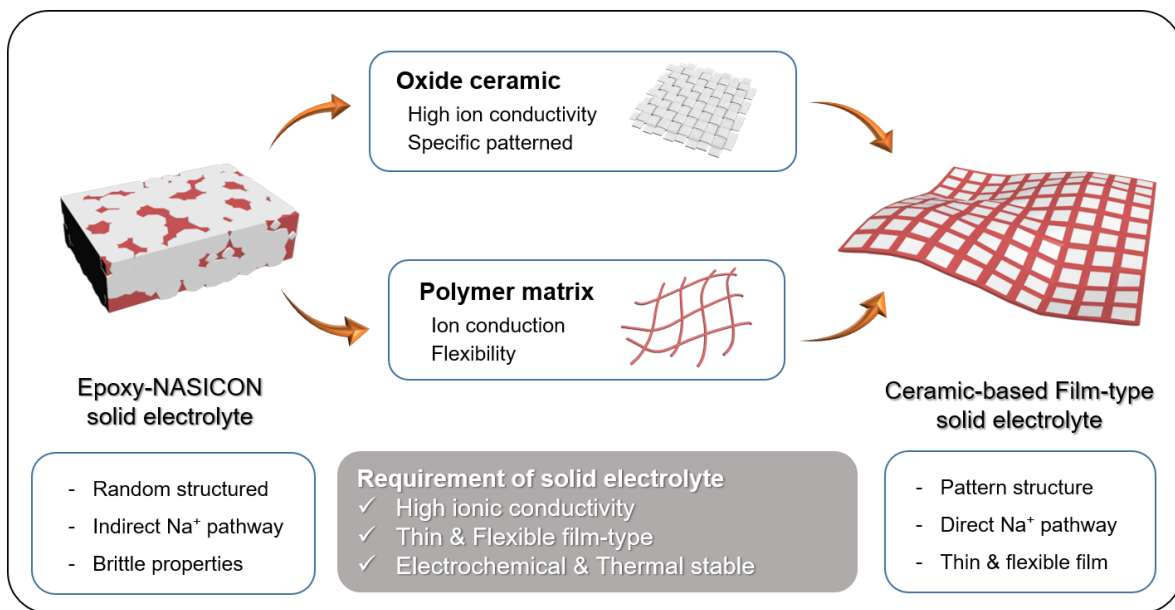


Figure 26. Suggest research directions for solid electrolytes in the future.

3.2. Patterned sintering oxide ceramic for the thin and flexible solid electrolyte

3.2.1. Ceramic sintered as specific pattern with sacrificial template

The oxide-based solid electrolyte used so far has been used only as a solid pellet-type ceramic. In order to increase the ionic conductivity of the solid electrolyte, a sintering process is performed. Since this process is performed at a high temperature, it can be manufactured only in a simple form. As a result, there were few applications that could be used, and there was not much demand for oxide-based solid electrolytes. However, recently, as research into making a solid electrolyte by combining an oxide-based solid electrolyte and a polymer material has progressed, the demand for the oxide-based solid electrolyte has increased, and at the same time, it has become necessary to manufacture the desired type. There is a need for a method of sintering ceramics with specific patterns that may have physical characteristics while forming more direct ion transport channels.

Various shapes are discussed as a specific pattern. First, after sintering, there is a need for a shape that can reduce the brittle properties of the ceramic itself. One of the examples is the existing commercially available Alumina fabric. Alumina fabric is a figure in which Al_2O_3 ceramic material is pulled out like a thin thread and woven into a fabric. Individual Al_2O_3 ceramics are still brittle and hard, but the entire fabric, woven in thin fabrics, can have flexible characteristics like a regular fabric. It is hard to be individually broken and easy to break, but if it can be made only in a specific pattern, it can be used in the form of a sufficiently flexible membrane. It is also important to note that in order to maximize the ion conducting effect of ceramics, it is necessary to create the most optimal ion transport channel. When making a film form in combination with a polymer, a method of sintering ceramics in the form of a mosaic is also considered so that the ceramic ion transport channel is made in the vertical direction of the film.

It can also be seen indirectly through the rule of mixture model described above that the physical properties are improved by compounding substances having a specific pattern. In the case of the existing rule of mixture, it was possible to calculate the physical property change when two substances were mixed at random. Accordingly, the researchers made a model including the shape, orientation, and elastic properties of each material in order to make corrections close to the actual model. In the case of the Halpin-Tsai model, it is calculated on the assumption that the materials to be mixed are perfectly aligned in one direction. In the case of the Chamis model, the elastic property of the compound to be compounded is included in the calculation formula to quantify it. There is also a Finite element method (FEM) that estimates physical properties like real models, including both of the following properties. When the various models are put together, the minimum intensity value that the mixed object can have is increased when the materials having a specific direction and shape are also mixed in a calculated value. (Figure 27) Even through this, if the actual ceramic is used after patterned sintering, an increase in physical strength can be expected.

Until now, the sintering method is to compress the ceramic powder under high pressure to form a pellet, and then to make the ceramic powder surfaces melt at each other at a high temperature of 1000°C or more. In this process, the void space between the powders is reduced and the ionic conductivity increases as the contact surface between ceramics increases. At this time, the ceramic crystal phase is formed more than just the physical bonding of the ceramic powder, so ion transfer through the ceramic is possible. However, in this way, it is difficult to make ceramics to the desired shape. Since the ceramic powders were randomly bonded to each other and the pores between the powders were not controllable, the final sintered form could only be produced in a simple pellet form. Therefore, it is necessary to devise another method to make the ceramic solid electrolyte sintered to the desired shape.

Recently, among the methods for producing a lithium ion solid electrolyte, various methods of making an oxide-based solid electrolyte into a specific shape have been studied. Basically, there is a method of sintering the ceramic internally by making a frame of a specific shape, and there is also a method of directly creating a desired shape using a 3D printing technique. However, since the sintering process of the oxide-based solid electrolyte passes a high temperature of 1000°C or more, a method of maintaining its shape after high temperature sintering is required.

The method used in this study was a method of sintering a solid electrolyte in the shape of a template using a carbon-based template after preparing a ceramic precursor of a complete solution. The template contains the liquid phase of ceramic precursor in its shape, and when the temperature is raised to sinter it, the carbon-based template is thermally decomposed and disappears at a specific temperature. (Figure 28) However, the retained ceramic solution is sintered as it is and retains its template form. If you check the result after the final sintering, you can see the sintered ceramic as it is in the shape of the template.

There are several types of carbon-based templates used in the experiment. The simplest is carbon cloth, which is woven into a carbon string and used as a fabric, and carbon felt, which is woven randomly in the form of a non-woven fabric. A company called Wizmac interwoven a single carbon string into multiple bundles and made a carbon cloth that weaves the bundles. In this study, carbon string, carbon cloth, carbon felt and Wizmac cloth were used as templates. Each sample can be confirmed through Figure 29. Before using each template impregnated with a ceramic precursor solution, it is necessary to check the temperature at which each sample undergoes pyrolysis. This is important information for adjusting the sintering temperature and heating step in using each template. As a result of the actual experiment, the TGA / DSC experiment of the carbon template (Figure 30) confirms the pyrolysis temperature, and the final pyrolysis temperature is different for each template. In the case of carbon felt, it is stable even up to 700 °C or more and then decomposed from around 800 °C. On the other hand, in the case of wizmac cloth, thermal decomposition starts from 500 °C, and if it exceeds 600 °C, all decomposes and disappears. Since the ceramic must maintain its shape at the temperature at which the template is thermally decomposed, it is necessary to keep the heating rate at the temperature as slow as

possible. The following diagram shows the sintering step used in practical application when using the wizmac carbon template.(Figure 31)

When the carbon-based template is impregnated with an ethanol-based solution, a ceramic precursor solution, the solution is sufficiently moistened with the template surface. The carbon template must not be used after removing the coating from the surface-coated template because the solution cannot penetrate sufficiently if there is a polymer coating on the surface of the material. After drying, the sufficiently moistened template is placed on the Pt plate and subjected to a heat treatment process according to the temperature step. If you check the change of the actual sample at each temperature, the carbon template starts to decompose from around 500 °C, and the white ceramic form remains sintered as the temperature increases.(Figure 32)

The shape of the ceramic after the final sintering can be confirmed directly by the eye, and it can be seen from the SEM image that the ceramic is sintered in the shape of the actual template. The carbon template of one strand is sintered with a thread-shaped ceramic, and the fabric template is sintered with a fabric-shaped ceramic. Indeed, one strand of ceramic is still brittle and weak. However, if multiple strands of ceramic are woven in the form of a fabric, the physical properties may be stronger. In addition, it is possible to add more flexible properties than conventional ceramics, so it can be expected to play a role as a solid electrolyte.(Figure 33)

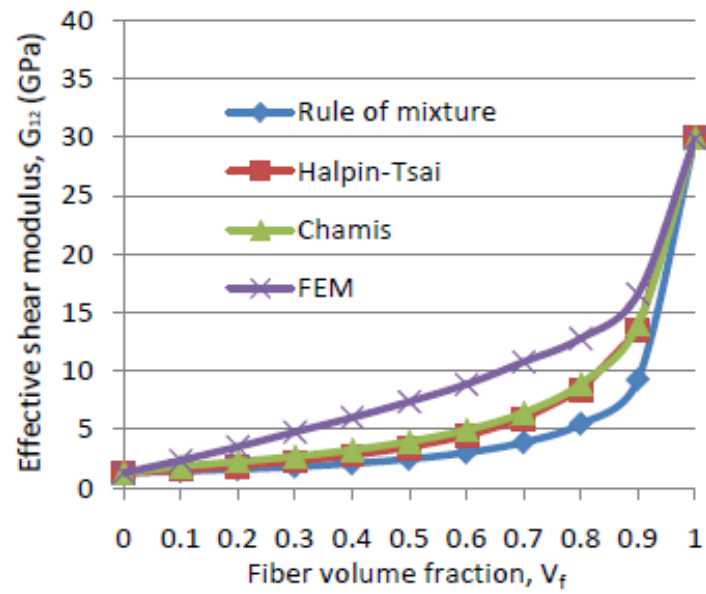


Figure 27. Various models of the rule of mixture and predicted values for lower bound calculation. It is possible to predict changes in physical properties of materials that are aligned.

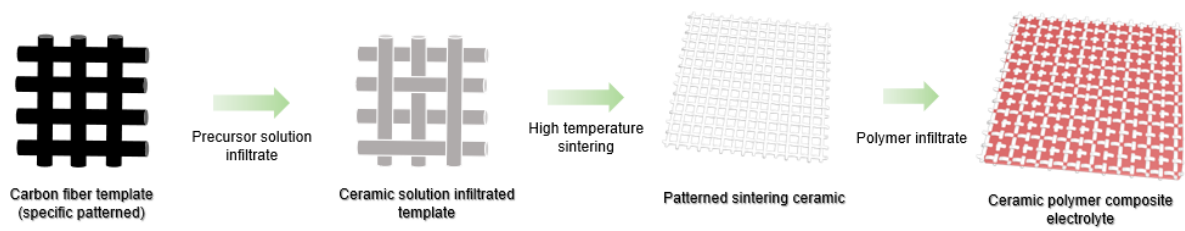
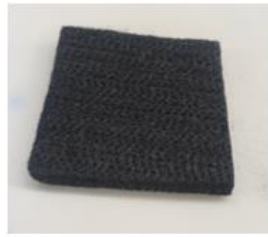


Figure 28. Schematic image of patterned ceramic solid electrolyte sintering method using template



< Carbon strand >



< Carbon felt >



< Carbon cloth >



< Carbon cloth(Wizmac) >

Figure 29. Actual appearance of each carbon template sample.

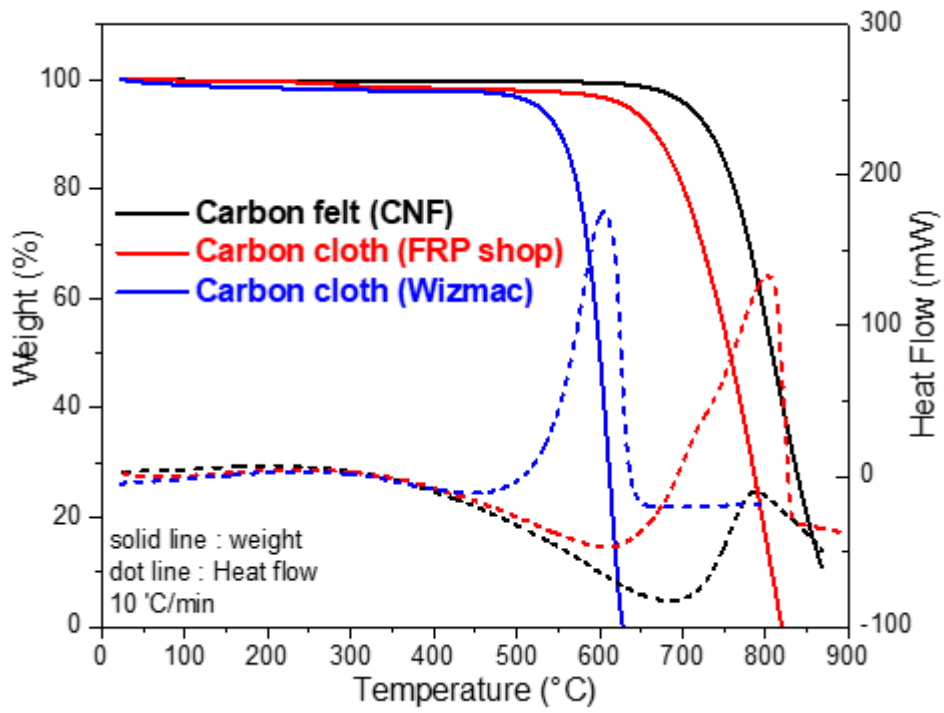


Figure 30. TGA/DSC result data of each carbon template sample from 25°C to 900°C.

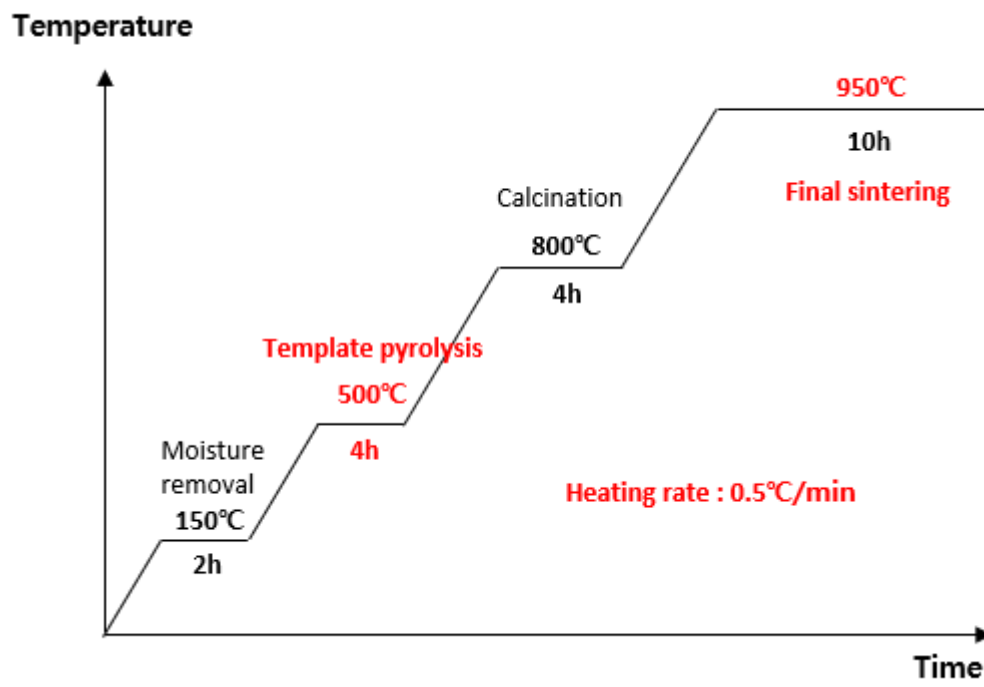


Figure 31. Heating step of carbon templated NASICON ceramic.

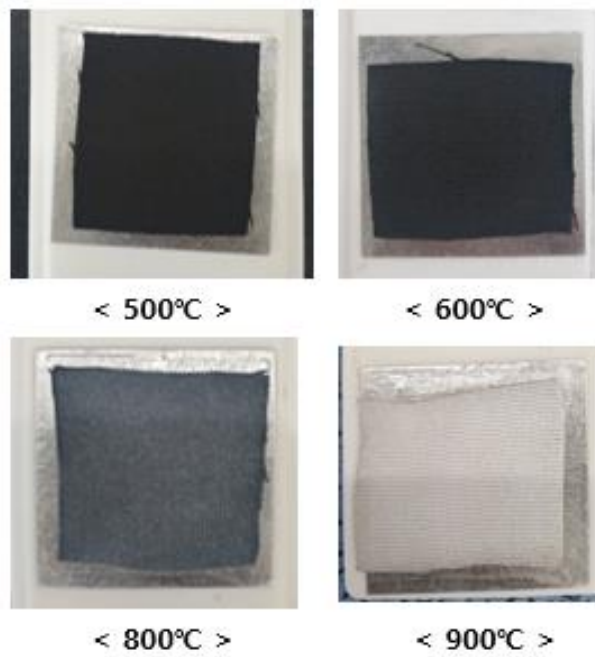


Figure 32. Variation by temperature of the carbon template sample impregnated with the actual ceramic precursor solution.

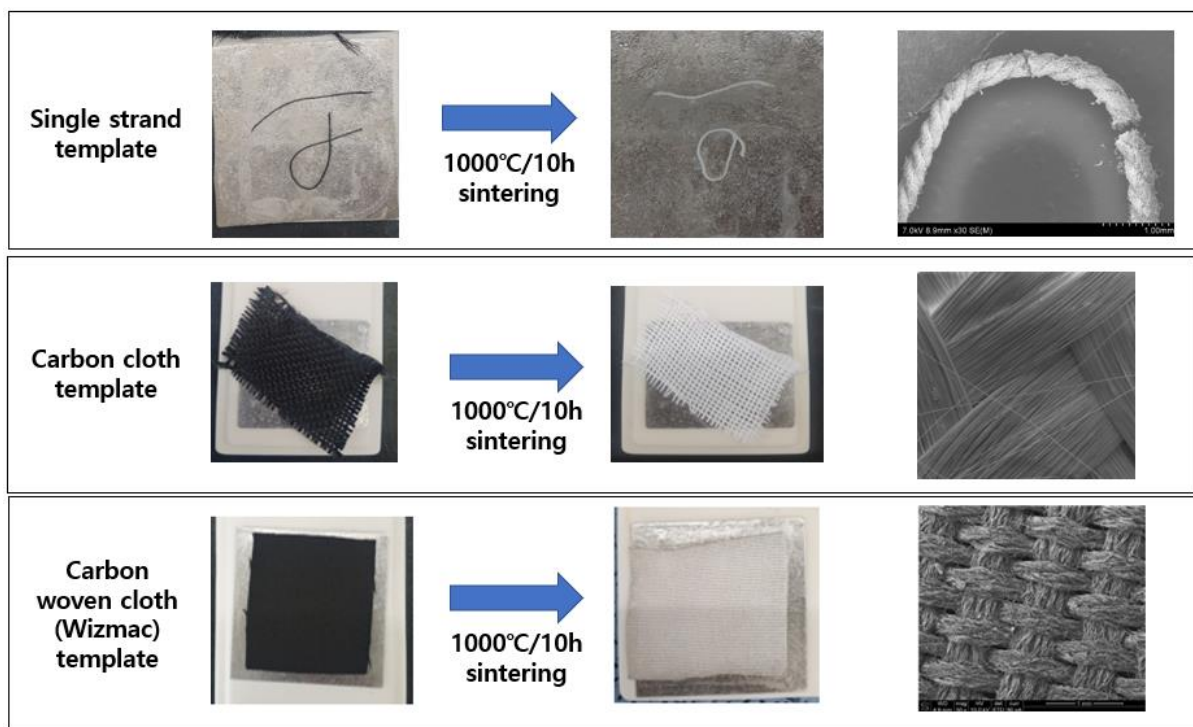


Figure 33. Comparison of the actual shape of each carbon template and the shape of the ceramic remaining after the final sintering

3.2.2. Mechanical properties of patterned ceramic based solid electrolyte

As described above, the ceramic solid electrolyte sintered in the form of a template has a lot of empty space inside as shown. Currently, the ceramic is sintered, so the physical strength is weak to use as an electrolyte, so the interior space is filled with a polymer material to produce a film type. This method is the same as the method of filling the former Epoxy polymer material into NASICON pellets. The liquid Epoxy-resin monomer material is impregnated into a patterned sintered ceramic, and then polymerized by heat. It can be made into a thin film. In the ceramic sintering sample using the Wizmac template, after adding an epoxy polymer, it comes out to a thickness of about 200 μm , and it can be made into a film of 100 μm thickness through a surface polishing process.

In the actual Wizmac carbon template, the thickness is about 300 ~ 400 μm . However, if the ceramic is impregnated and then sintered, the thickness is reduced by roughly half. Not only the thickness is reduced, but the overall shape shrinks a lot, and the sintering occurs because the template is decomposed and the place where the template disappears is sintered as the ceramic fills up. The thickness of one strand of carbon string before sintering was about 10 μm , but if you check the thickness after sintering, you can see the shrinkage of 5~6 μm .(Figure 34) It can be seen that the overall template form was maintained. According to the experiments to date, the shrinkage rate differs depending on the concentration of the prepared ceramic precursor solution, and the higher the concentration, the smaller the shrinkage rate appears to be. And another thing that could be confirmed is that the density of the final sintered ceramic is also determined according to the difference in the concentration of the ceramic precursor. In order to find the initial experimental conditions, when the template was impregnated with a dilute concentration of about 0.3 M, the shape remained after the final sintering, but the density of the ceramic was low, so that the crumb occurred easily. This can also be seen through the SEM of the Figure 35, where you can see that the ceramic has been sintered, leaving a lot of empty space around the place where the template was thermally decomposed. Finally, a ceramic precursor solution having a concentration of 1M was used to increase the sintering density of the ceramic as much as possible. The higher the ceramic precursor solution concentration, the more the void space inside the sintered ceramic decreased, and the physical strength also increased a lot.(Figure 36) The reason why the density of the sintered ceramic is important is that the final ion-transport channel is a ceramic solid electrolyte, so that the ion transfer effect is deteriorated as the density is low and there are more empty spaces. Since the physical strength also has a lower density, the strength becomes weaker, so it is necessary to increase the density of the patterned sintered ceramic by preparing an optimal high concentration solution.

By checking the cross-section of the final sintered patterned ceramic solid electrolyte, the ion transfer channel of the ion ceramic strand can be confirmed.(Figure 37) According to the shape of the currently used Wizmac carbon template, the ceramic solid electrolyte passage formed in a zigzag fabric form is not a vertical ion transfer effect, but bypasses it to create a direction through which ions can pass. The

remaining empty space can be filled with polymeric materials. The Figure 38 of filling the remaining empty space with Epoxy polymer material in the same way can be confirmed through the figure. EDS analysis can compare the ceramic material and the polymer material filled in the remaining space by C material analysis. Then, while maintaining the ion transport channel, the strength can be increased relatively, and it can be produced in the form of a thin film. Unlike sintering with ceramic powder before, since the shape of the ceramic can be adjusted, as many ion-transfer channels as desired can be formed and the rest can be used to enhance physical properties.(Figure 39)

Basically, the brittle nature of ceramics remains, but after polymer treatment, the solid electrolyte film can be seen to be more flexible than conventional ceramics. The patterned epoxy-NASICON solid electrolyte after treatment of about 200 μm thick Epoxy polymer can measure bending properties. The sample sintered with the previous NASICON powder showed the property of breaking immediately without any bending property, but in the case of the patterned epoxy-NASICON, it was thin enough to have a bending property. The same sample 4 x 4 cm area, 200 μm thick samples were wrapped in acrylic cylinders of different diameters, and the bending characteristics were checked while showing resilience. The actual bending shape from 5cm to 1cm diameter cylinders was compared and can be confirmed through the Figure 40. It was confirmed that the physical properties of the current Epoxy-NASICON sample can be sufficiently recovered after bending up to a 2 cm diameter cylinder, and cracking occurs below. This is a value that approximates the flexibility characteristics of the present oxide-based solid electrolyte and is expected to be sufficiently utilized in the future.

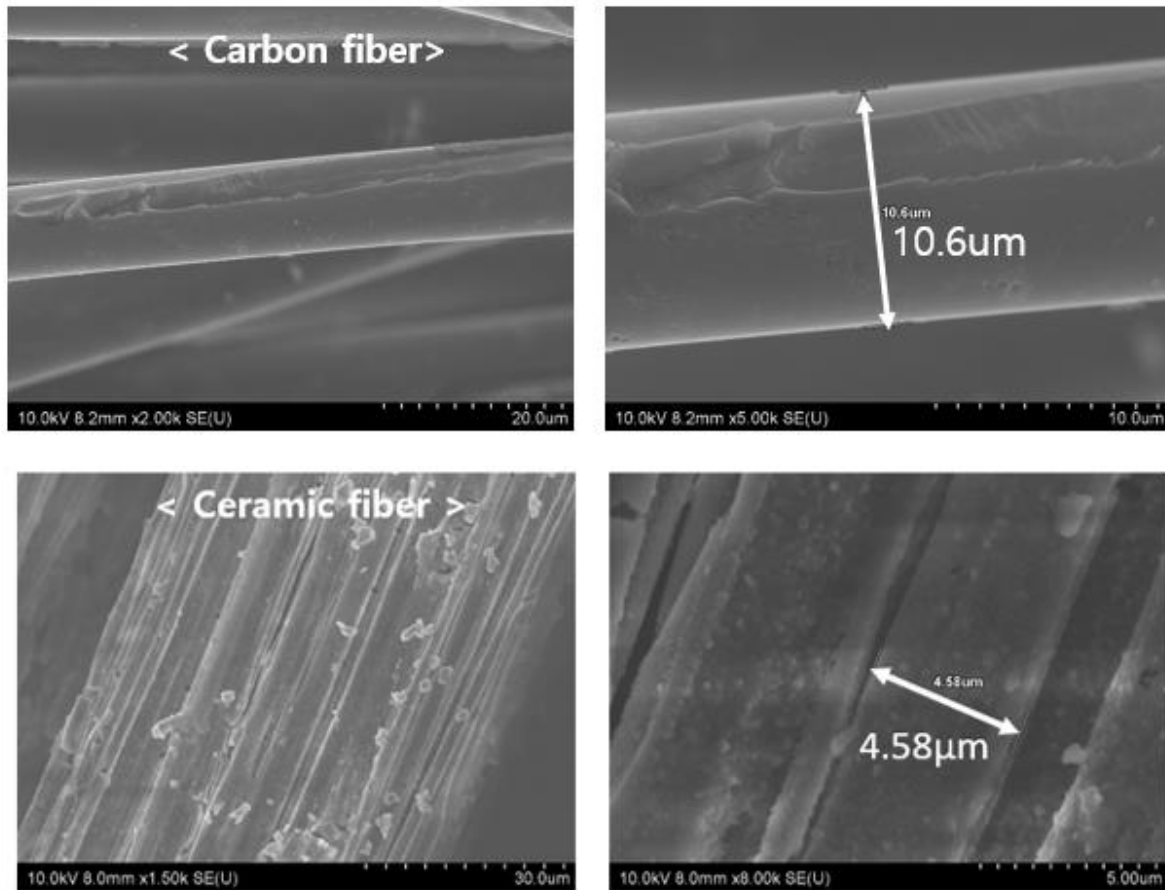
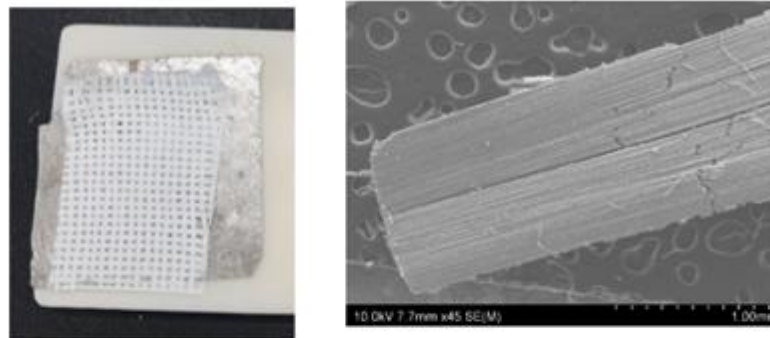


Figure 34. SEM image and thickness of a single strand of carbon fiber. SEM image of the ceramic solid electrolyte finally sintered using the carbon fiber.



< 0.3M solution ceramic >

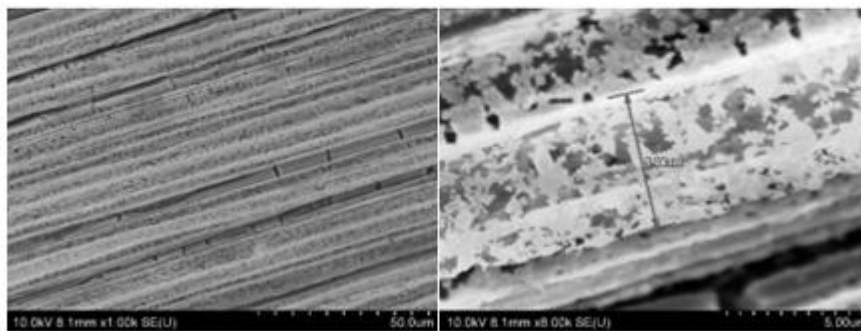


Figure 35. Patterned ceramic sintered at a concentration of 0.3 M ceramic precursor. After the final sintering, it can be confirmed that the ceramic inner density is low.

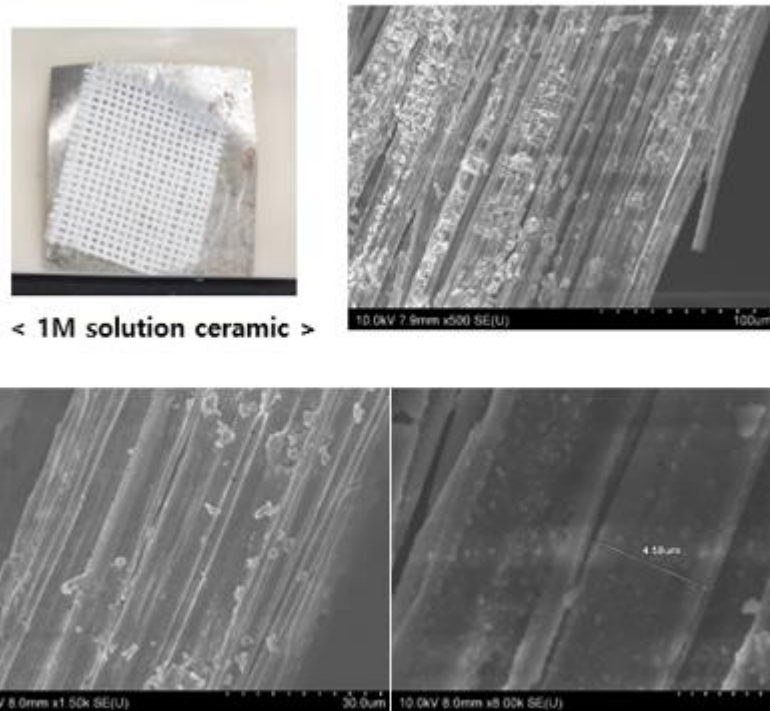


Figure 36. Patterned ceramic sintered at a ceramic precursor concentration of 1 M. After the final sintering, it is possible to check the high internal density of the ceramic.

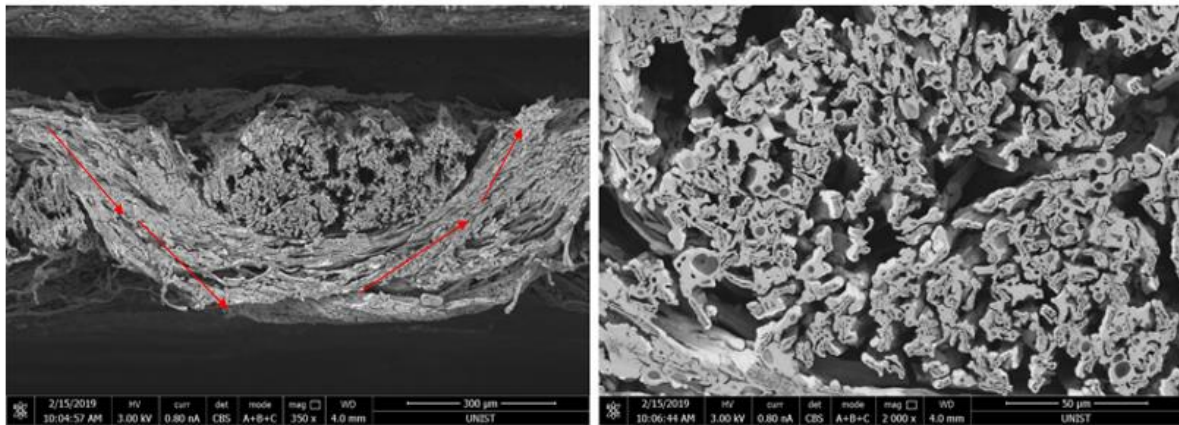


Figure 37. Cross-section SEM image of the final sintered NASICON ceramic using Wizmac template. The sintering of ceramics capable of ion transfer in a zigzag shape.

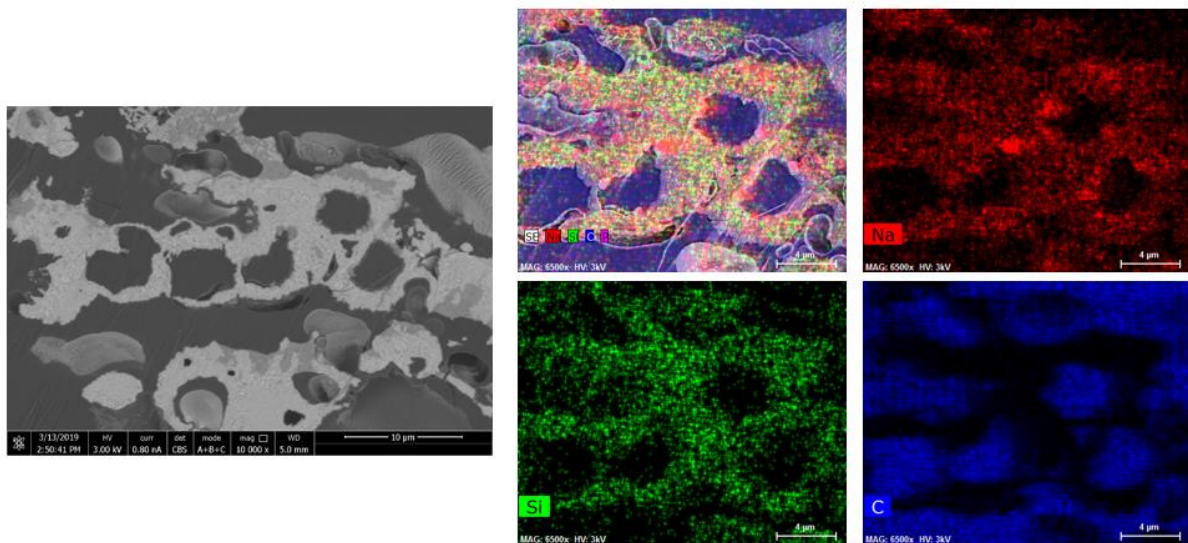


Figure 38. Epoxy-NASICON SEM cross-section image with Epoxy polymer added to patterned sintered NASICON ceramics and EDS analysis results.

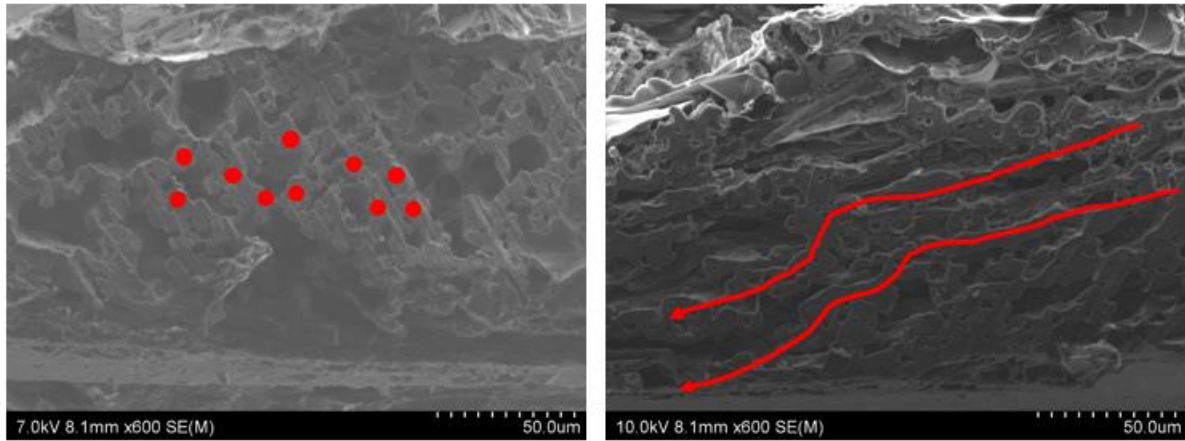


Figure 39. Cross-sectional SEM image of Epoxy-NASICON solid electrolyte. Ion transfer channel through ceramic can be checked.

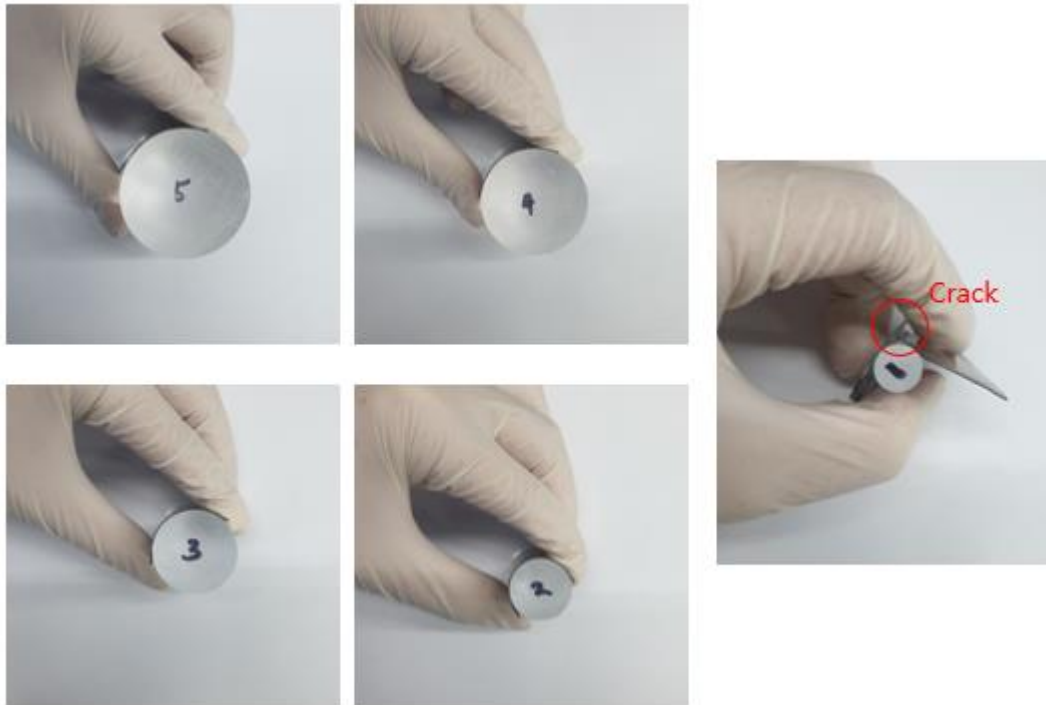


Figure 40. Testing the bending properties using an acrylic cylinder. Experiments with cylinders 5 to 1 cm in diameter.

3.2.3. Electrochemical characterization

The electrochemical properties can be said to be like the previous epoxy-NASICON samples. Basically, since NASICON and Epoxy polymer materials have not been changed, the original thermal stability and electrochemical stability are maintained. Figure 41 and Figure 42 shows the results of TGA and LSV experiments. If you check it through TGA, you can see a stable appearance until epoxy decomposes at 400 °C. Even when comparing the electrochemical stability through LSV, it is stable up to 6V. The electrochemical stability of epoxy-NASICON solid electrolytes is higher than that of existing liquid electrolytes and ionic liquids, which exhibit reactivity at 4.5V and 5.0V. However, the electrochemical stability is lower than that of the previous Epoxy-NASICON in the form of pellets. It seems that the characteristics of the polymer appear as the proportion of the ceramic decreases and the proportion of the polymer increases as the ceramic sintering is patterned.

The results of measuring ion conduction through EIS analysis can be confirmed through the Figure 43. The ionic conductivity measured through experiments to date is about 10^{-5} Scm^{-1} . It has a low ionic conductivity compared to the epoxy-NASICON in the previous pellet state, which is presumed since there are not many channels through which ions can pass. In addition, it is necessary to study ceramic sintering conditions and patterns of solid electrolytes that can exhibit optimal ion transport. In the case of the ceramic template using the present Wizmac carbon template, since the fabric is woven in a zigzag form, the sintered ceramic is also in a zigzag form. The best form is that the ceramic solid electrolyte is sintered in the vertical direction of the final solid electrolyte and fills other spaces with the polymer to enhance the physical properties. In this regard, research directions for future templates are needed.

Other polymer materials may be used in addition to the epoxy polymer. Epoxy polymers are not ion-conducting polymers, so they only increase their physical properties. However, if an ion-conducting polymer is used, an additional ion transfer effect can be expected. The polymer material used as a test is a material that is mixed with Trimethylolpropane ethoxylate triacrylate (ETPTA) polymer and Na salt and then cured using UV radiation. When the above polymer electrolyte was used alone, it showed ionic conductivity of about $1.2 \times 10^{-5} \text{ S cm}^{-1}$ at room temperature, but it was expected that it could show better performance when combined with the aligned ceramic solid electrolyte. Indeed, because of applying ETPTA UV curing polymer electrolyte to the patterned NASICON solid electrolyte, better ion conductivity values could be confirmed. If you look at the ion conductivity through EIS measurement through the Figure 44, you can see that the ion conductivity increased up to $1.0 \times 10^{-4} \text{ S cm}^{-1}$. Physical properties also have flexible properties and can be used as thin film solid electrolytes. It can be applied to cell assembly more easily than the existing pellet type solid electrolyte.

It can be applied to cell assembly more easily than the existing pellet type solid electrolyte. The half-cell using the NVP anode and Na metal, which was previously manufactured, was also applied as a patterned ceramic solid electrolyte. When the cell performance was viewed with a current value of 0.1

C-rate at room temperature, it was confirmed that the capacity of 120mAh/g and the stable state of 20 cycles or more were observed. Figure 45 shows the cell performance and cycle data. Through this, it is confirmed that the cell characteristics can be sufficiently observed even with a solid electrolyte based on an oxide-based ceramic.

Up to now, the pattern of the oxide-based solid electrolyte was used only as a template in the form of a usable fabric, but in the future, if a desired type of template is applied, various types of solid electrolytes may be produced. As mentioned earlier, when a solid electrolyte and a polymer material are used in combination, a solid electrolyte type capable of showing an optimal ion transfer effect is required. It is an optimal condition that the solid electrolyte is sintered in the vertical direction of the film, and the rest of the film is a polymer having good bonding properties, thereby increasing physical strength. If an ion-conducting polymer material is additionally used, it may have a more efficient ion conductivity.

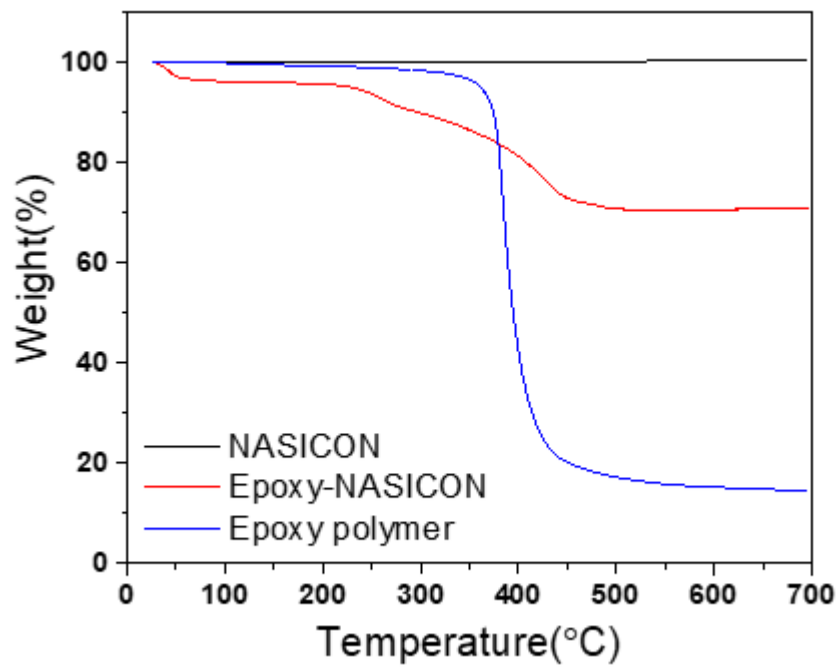


Figure 41. TGA analysis results of basic NASICON ceramic, epoxy polymer, and patterned sintered epoxy-NASICON samples.

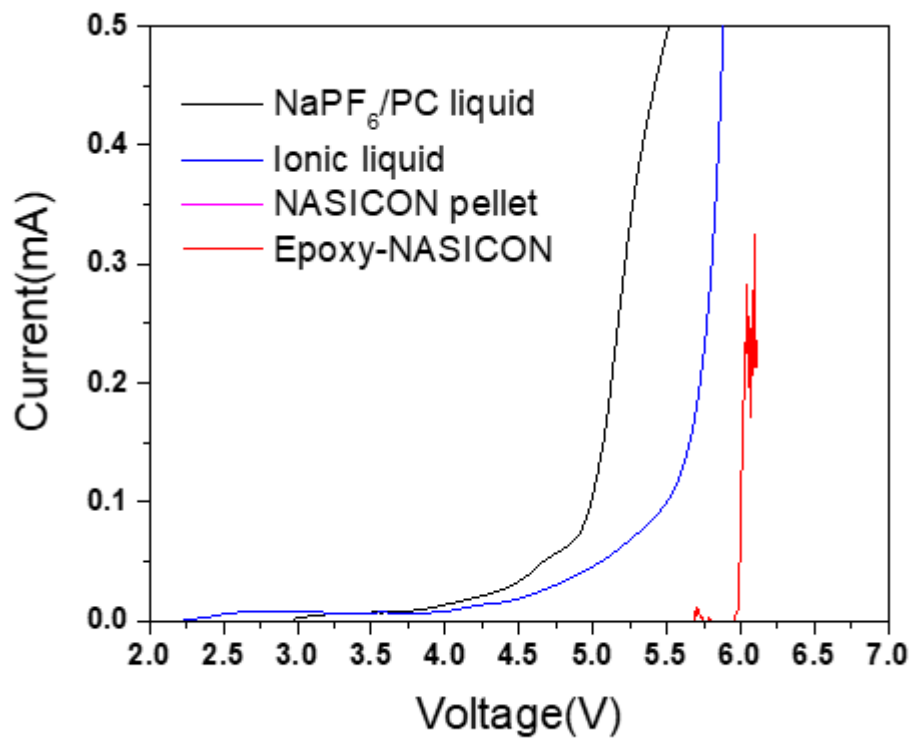


Figure 42. Electrochemical stability analysis through LSV test of each sample.

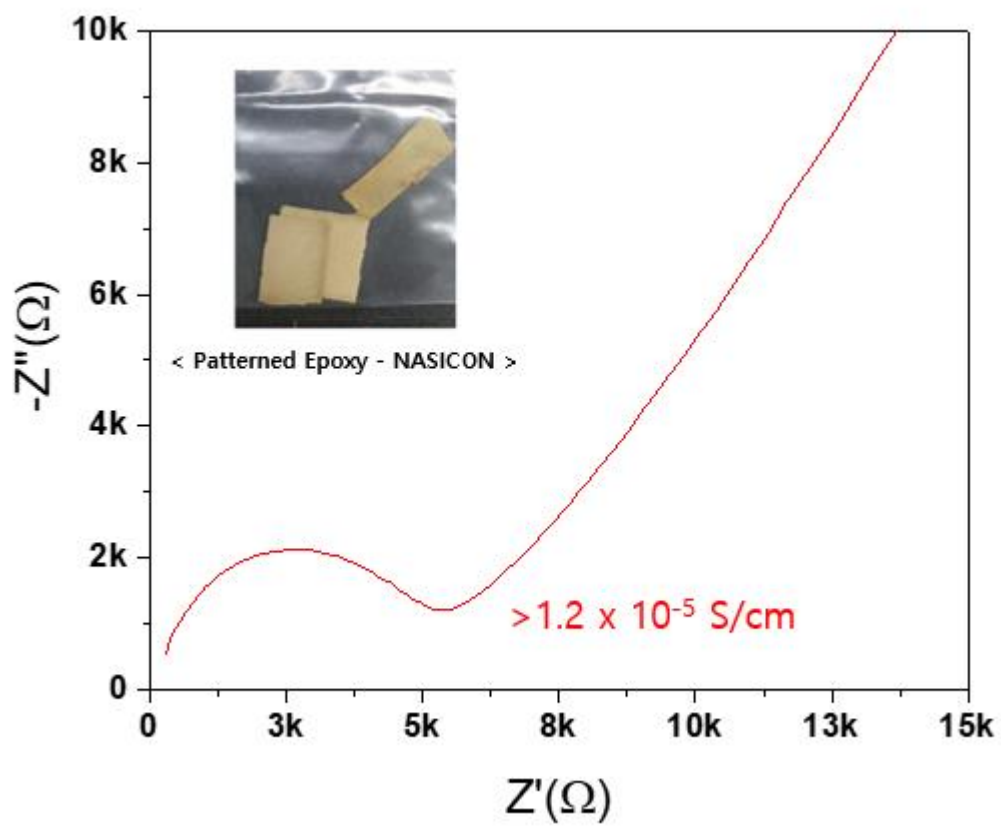


Figure 43. The appearance of the patterned sintered epoxy-NASICON sample and the result of ion conductivity measurement through EIS analysis.



< Patterned NASICON + UV polymer >

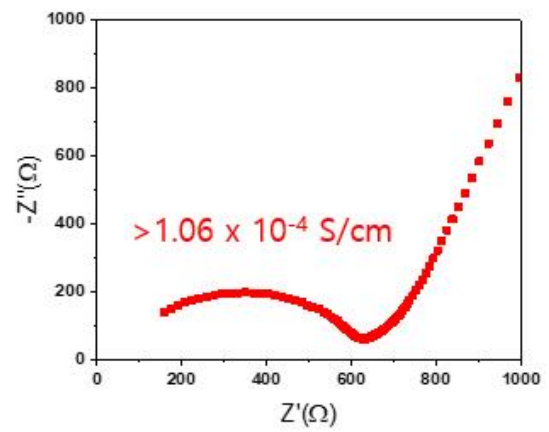


Figure 44. Measurement of ion conductivity through analysis of solid electrolyte and EIS by applying UV curing ETPTA polymer to patterned sintered NASICON.

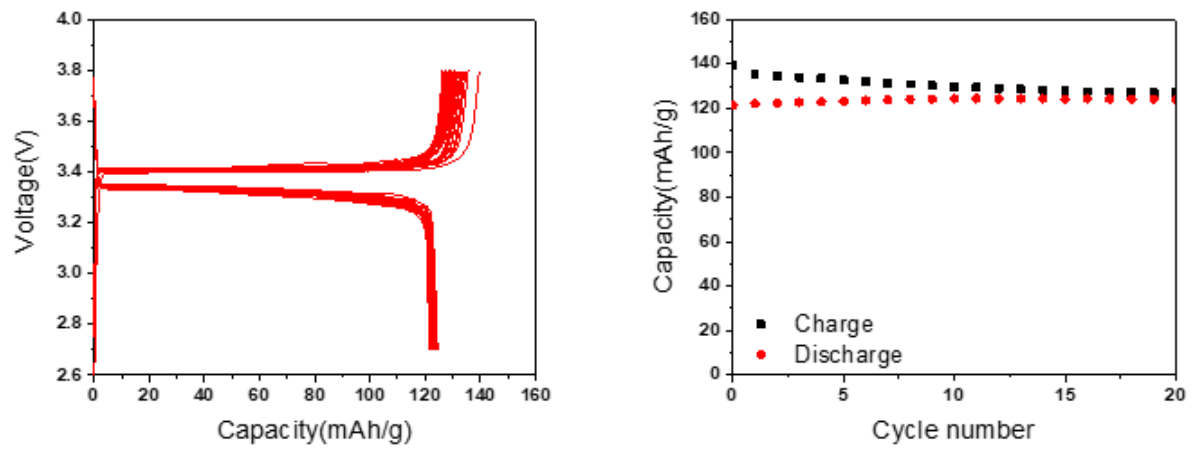


Figure 45. Na / NVP half-cell performance and cycle graph made using patterned sintered NASICON solid electrolyte.

V. Conclusion

This is the result of research on methods that can be applied to Na-ion battery systems using oxide-based ceramic solid electrolytes. For Li-ion batteries and Na-ion batteries, stability is a top priority to meet current high-capacity ESS standards. In the secondary battery system using an existing organic liquid electrolyte, many studies have been attempted to solve this stability since the issue of instability, which is easily burned, remains. Among them, a solid electrolyte is being researched as an alternative material that can replace the existing liquid electrolyte. Among them, an oxide-based solid electrolyte that is thermally stable in the air is spotlighted as a substitute material. However, the disadvantage of the oxide-based solid electrolyte is that due to the high interfacial resistance between the solid powders, it is impossible to expect a normal ion transfer effect through simple physical contact. For this reason, various studies have been conducted on a method of utilizing an oxide-based solid electrolyte. So far, the ion conducting effect of the solid electrolyte was expected by mixing the oxide-based solid electrolyte powder and the polymer electrolyte. At the same time, thermal stability, and electrochemical stability, which are advantages of the oxide-based solid electrolyte, could be expected. However, in the composite electrolyte using an oxide-based solid electrolyte powder, the proportion of ceramics has not exceeded 50% or more. It was confirmed through the oxide-based solid electrolyte that the ion conducting effect was hardly in the powder state, so that the proportion of the ceramic could not be increased. This is because the ionic conductivity drops rapidly when the ceramic ratio exceeds 50%. Therefore, it is difficult to expect thermal stability and electrochemical stability.

Therefore, to transfer ions through an oxide-based solid electrolyte, it is necessary to form an ion transfer channel through sintering. After the high-temperature sintering process, the ceramic surface melts and the interface resistance disappears. However, it was difficult to utilize the sintering process because it was made only in the form of thick and brittle pellets. There is a need for a method to increase the physical strength after sintering and make it thin.

A method of manufacturing a thin solid electrolyte was devised by filling the internal pores or voids of the sintered ceramic solid electrolyte with a polymer material capable of increasing physical strength. It was confirmed that the present pellet-type solid electrolyte was intentionally increased in porosity and sintered, and the higher the polymer material was filled, the higher the strength. However, this method is difficult to use in a sufficiently thin form. Additional features are needed because there are still fragile features. The ceramic solid electrolyte should provide a channel through which ions can be transferred, and at the same time, reduce physical properties that break. As a solution, a patterned ceramic solid electrolyte sintering method using a template is proposed. Currently, the possibility of sintering a ceramic solid electrolyte in the form of a template using a carbon-based fabric type template was confirmed. Using the solid electrolyte thus prepared, a thermally stable solid electrolyte up to 400 °C and an electrochemically stable solid electrolyte up to 6V or higher was produced. Using the above

solid electrolyte, the capacity of 120mAh/g and stable cell performance up to 20 cycles can be seen in the half cell using NVP anode and Na metal. It is considered that the above research direction is necessary to utilize the oxide-based solid electrolyte in the future. It has been confirmed that there is no longer an ion transfer effect with the oxide-based solid electrolyte powder, and after sintering, a specific type of sintering method is required to supplement physical properties. The sintering method using the present template is highly likely to be used in the future because various types of ceramics can be sintered by using a template of a desired shape. Through this, we expect to develop a stable Na-ion battery market.

Reference

1. Goodenough, J. B.; Kim, Y. J. C. o. m., Challenges for rechargeable Li batteries. **2010**, *22* (3), 587-603.
2. Tarascon, J.-M.; Armand, M., Issues and challenges facing rechargeable lithium batteries. In *Materials for sustainable energy: a collection of peer-reviewed research and review articles from Nature Publishing Group*, World Scientific: 2011; pp 171-179.
3. Scrosati, B.; Garche, J. J. J. o. p. s., Lithium batteries: Status, prospects and future. **2010**, *195* (9), 2419-2430.
4. Li, M.; Lu, J.; Chen, Z.; Amine, K. J. A. M., 30 years of lithium-ion batteries. **2018**, *30* (33), 1800561.
5. He, P.; Yu, H.; Zhou, H. J. J. o. M. C., Layered lithium transition metal oxide cathodes towards high energy lithium-ion batteries. **2012**, *22* (9), 3680-3695.
6. Croguennec, L.; Palacin, M. R. J. J. o. t. A. C. S., Recent achievements on inorganic electrode materials for lithium-ion batteries. **2015**, *137* (9), 3140-3156.
7. Ellis, B. L.; Lee, K. T.; Nazar, L. F. J. C. o. m., Positive electrode materials for Li-ion and Li-batteries. **2010**, *22* (3), 691-714.
8. Tarascon, J.-M. J. N. c., Is lithium the new gold? **2010**, *2* (6), 510-510.
9. Pan, H.; Hu, Y.-S.; Chen, L. J. E.; Science, E., Room-temperature stationary sodium-ion batteries for large-scale electric energy storage. **2013**, *6* (8), 2338-2360.
10. Zu, C.-X.; Li, H. J. E.; Science, E., Thermodynamic analysis on energy densities of batteries. **2011**, *4* (8), 2614-2624.
11. De La Llave, E.; Borgel, V.; Park, K.-J.; Hwang, J.-Y.; Sun, Y.-K.; Hartmann, P.; Chesneau, F.-F.; Aurbach, D. J. A. a. m.; interfaces, Comparison between Na-ion and Li-ion cells: understanding the critical role of the cathodes stability and the anodes pretreatment on the cells behavior. **2016**, *8* (3), 1867-1875.
12. Slater, M. D.; Kim, D.; Lee, E.; Johnson, C. S. J. A. F. M., Sodium-ion batteries. **2013**, *23* (8), 947-958.
13. David, L.; Thomas, R., *Linden's Handbook of Batteries 3*. McGraw-Hill Education: 2010.
14. Hwang, J.-Y.; Myung, S.-T.; Sun, Y.-K., Sodium-ion batteries: present and future. *Chemical Society reviews* **2017**, *46* (12), 3529-3614.
15. Adelhelm, P.; Hartmann, P.; Bender, C. L.; Busche, M.; Eufinger, C.; Janek, J. J. B. j. o. n., From lithium to sodium: cell chemistry of room temperature sodium–air and sodium–sulfur batteries. **2015**, *6* (1), 1016-1055.

16. Mizushima, K.; Jones, P.; Wiseman, P.; Goodenough, J. B. J. M. R. B., Li_xCoO_2 ($0 < x < 1$): A new cathode material for batteries of high energy density. **1980**, *15* (6), 783-789.
17. Nagelberg, A. S.; Worrell, W. L. J. J. o. S. S. C., A thermodynamic study of sodium-intercalated TaS₂ and TiS₂. **1979**, *29* (3), 345-354.
18. Delmas, C.; Fouassier, C.; Hagenmuller, P. J. P. B. c., Structural classification and properties of the layered oxides. **1980**, *99* (1-4), 81-85.
19. Braconnier, J.-J.; Delmas, C.; Fouassier, C.; Hagenmuller, P. J. M. R. B., Comportement electrochimique des phases Na_xCoO_2 . **1980**, *15* (12), 1797-1804.
20. Whittingham, M. S. J. P. i. S. S. C., Chemistry of intercalation compounds: metal guests in chalcogenide hosts. **1978**, *12* (1), 41-99.
21. Kubota, K.; Komaba, S. J. J. o. T. E. S., practical issues and future perspective for Na-ion batteries. **2015**, *162* (14), A2538-A2550.
22. Hwang, J.-Y.; Myung, S.-T.; Sun, Y.-K. J. C. S. R., Sodium-ion batteries: present and future. **2017**, *46* (12), 3529-3614.
23. Ponrouch, A.; Monti, D.; Boschini, A.; Steen, B.; Johansson, P.; Palacín, M. R., Non-aqueous electrolytes for sodium-ion batteries. *Journal of Materials Chemistry A* **2015**, *3* (1), 22-42.
24. Kato, Y.; Hori, S.; Saito, T.; Suzuki, K.; Hirayama, M.; Mitsui, A.; Yonemura, M.; Iba, H.; Kanno, R. J. N. E., High-power all-solid-state batteries using sulfide superionic conductors. **2016**, *1* (4), 1-7.
25. Jung, K. N.; Shin, H. S.; Park, M. S.; Lee, J. W. J. C., Solid-State Lithium Batteries: Bipolar Design, Fabrication, and Electrochemistry. **2019**, *6* (15), 3842-3859.
26. Yang, J.; Zhang, H.; Zhou, Q.; Qu, H.; Dong, T.; Zhang, M.; Tang, B.; Zhang, J.; Cui, G., Safety-Enhanced Polymer Electrolytes for Sodium Batteries: Recent Progress and Perspectives. *ACS applied materials & interfaces* **2019**, *11* (19), 17109-17127.
27. Kamaya, N.; Homma, K.; Yamakawa, Y.; Hirayama, M.; Kanno, R.; Yonemura, M.; Kamiyama, T.; Kato, Y.; Hama, S.; Kawamoto, K.; Mitsui, A., A lithium superionic conductor. *Nature Materials* **2011**, *10* (9), 682-686.
28. Kato, Y.; Hori, S.; Saito, T.; Suzuki, K.; Hirayama, M.; Mitsui, A.; Yonemura, M.; Iba, H.; Kanno, R., High-power all-solid-state batteries using sulfide superionic conductors. *Nature Energy* **2016**, *1* (4), 16030.
29. Hayashi, A.; Noi, K.; Sakuda, A.; Tatsumisago, M. J. N. c., Superionic glass-ceramic electrolytes for room-temperature rechargeable sodium batteries. **2012**, *3* (1), 1-5.
30. Chu, I.-H.; Kompella, C. S.; Nguyen, H.; Zhu, Z.; Hy, S.; Deng, Z.; Meng, Y. S.; Ong, S. P. J. S. r., Room-temperature all-solid-state rechargeable sodium-ion batteries with a Cl-doped Na₃PS₄ superionic conductor. **2016**, *6*, 33733.
31. Wang, H.; Chen, Y.; Hood, Z. D.; Sahu, G.; Pandian, A. S.; Keum, J. K.; An, K.; Liang, C. J. A. C. I. E., An Air-Stable Na₃SbS₄ Superionic Conductor Prepared by a Rapid and Economic Synthetic Procedure. **2016**, *55* (30), 8551-8555.

32. Banerjee, A.; Park, K. H.; Heo, J. W.; Nam, Y. J.; Moon, C. K.; Oh, S. M.; Hong, S. T.; Jung, Y. S. J. A. C. I. E., Na₃SbS₄: A Solution Processable Sodium Superionic Conductor for All-Solid-State Sodium-Ion Batteries. **2016**, *55* (33), 9634-9638.
33. Zhang, L.; Zhang, D.; Yang, K.; Yan, X.; Wang, L.; Mi, J.; Xu, B.; Li, Y. J. A. s., Vacancy-Contained Tetragonal Na₃SbS₄ Superionic Conductor. **2016**, *3* (10), 1600089.
34. Duchardt, M.; Ruschewitz, U.; Adams, S.; Dehnen, S.; Roling, B. J. A. C. I. E., Vacancy-Controlled Na⁺ Superion Conduction in Na₁₁Sn₂PS₁₂. **2018**, *57* (5), 1351-1355.
35. Zhang, Z.; Ramos, E.; Lalère, F.; Assoud, A.; Kaup, K.; Hartman, P.; Nazar, L. F. J. E.; Science, E., Na₁₁Sn₂PS₁₂: a new solid state sodium superionic conductor. **2018**, *11* (1), 87-93.
36. Wang, N.; Yang, K.; Zhang, L.; Yan, X.; Wang, L.; Xu, B. J. J. o. M. S., Improvement in ion transport in Na₃PSe₄-Na₃SbSe₄ by Sb substitution. **2018**, *53* (3), 1987-1994.
37. Li, J.; Ma, C.; Chi, M.; Liang, C.; Dudney, N. J. J. A. E. M., Solid electrolyte: the key for high-voltage lithium batteries. **2015**, *5* (4), 1401408.
38. Neudecker, B.; Dudney, N.; Bates, J. J. J. o. t. E. S., "Lithium-Free" Thin-Film Battery with In Situ Plated Li Anode. **2000**, *147* (2), 517.
39. Ohtomo, T.; Hayashi, A.; Tatsumisago, M.; Kawamoto, K., All-solid-state batteries with Li₂O-Li₂S-P₂S₅ glass electrolytes synthesized by two-step mechanical milling. *Journal of Solid State Electrochemistry* **2013**, *17* (10), 2551-2557.
40. Zhu, Y.; He, X.; Mo, Y. J. J. o. M. C. A., First principles study on electrochemical and chemical stability of solid electrolyte-electrode interfaces in all-solid-state Li-ion batteries. **2016**, *4* (9), 3253-3266.
41. Bates, J.; Dudney, N.; Gruzalski, G.; Zuhr, R.; Choudhury, A.; Luck, C.; Robertson, J. J. S. s. i., Electrical properties of amorphous lithium electrolyte thin films. **1992**, *53*, 647-654.
42. Yu, X.; Bates, J.; Jellison Jr, G.; Hart, F. J. J. o. t. e. s., A stable thin-film lithium electrolyte: lithium phosphorus oxynitride. **1997**, *144* (2), 524.
43. Inaguma, Y.; Liqun, C.; Itoh, M.; Nakamura, T.; Uchida, T.; Ikuta, H.; Wakihara, M. J. S. S. C., High ionic conductivity in lithium lanthanum titanate. **1993**, *86* (10), 689-693.
44. Aono, H.; Sugimoto, E.; Sadaoka, Y.; Imanaka, N.; Adachi, G. y. J. J. o. t. e. s., Ionic conductivity of solid electrolytes based on lithium titanium phosphate. **1990**, *137* (4), 1023-1027.
45. Kahlaoui, R.; Arbi, K.; Sobrados, I.; Jimenez, R.; Sanz, J.; Ternane, R. J. I. c., Cation Miscibility and Lithium Mobility in NASICON Li_{1+x}Ti_{2-x}Sc_x(PO₄)₃ (0 ≤ x ≤ 0.5) Series: A Combined NMR and Impedance Study. **2017**, *56* (3), 1216-1224.
46. Murugan, R.; Thangadurai, V.; Weppner, W. J. A. C. I. E., Fast lithium ion conduction in garnet-type Li₇La₃Zr₂O₁₂. **2007**, *46* (41), 7778-7781.

47. Kotobuki, M.; Munakata, H.; Kanamura, K.; Sato, Y.; Yoshida, T. *J. J. o. T. E. S.*, Compatibility of Li₇La₃Zr₂O₁₂ solid electrolyte to all-solid-state battery using Li metal anode. **2010**, *157* (10), A1076-A1079.
48. Lu, X.; Xia, G.; Lemmon, J. P.; Yang, Z. *J. J. o. P. S.*, Advanced materials for sodium-beta alumina batteries: Status, challenges and perspectives. **2010**, *195* (9), 2431-2442.
49. Hueso, K. B.; Armand, M.; Rojo, T. J. E.; Science, E., High temperature sodium batteries: status, challenges and future trends. **2013**, *6* (3), 734-749.
50. Yang, Z.; Zhang, J.; Kintner-Meyer, M. C.; Lu, X.; Choi, D.; Lemmon, J. P.; Liu, J. J. C. r., Electrochemical energy storage for green grid. **2011**, *111* (5), 3577-3613.
51. Mauvy, F.; Siebert, E.; Fabry, P. J. T., Reactivity of NASICON with water and interpretation of the detection limit of a NASICON based Na⁺ ion selective electrode. **1999**, *48* (2), 293-303.
52. Fuentes, R.; Figueiredo, F.; Marques, F.; Franco, J. J. S. S. I., Reaction of NASICON with water. **2001**, *139* (3-4), 309-314.
53. Radhakrishnan, B.; Ong, S. P. J. F. i. E. R., Aqueous stability of alkali superionic conductors from first-principles calculations. **2016**, *4*, 16.
54. Goodenough, J. B.; Hong, H.-P.; Kafalas, J. J. M. R. B., Fast Na⁺-ion transport in skeleton structures. **1976**, *11* (2), 203-220.
55. Hong, H.-P. J. M. R. B., Crystal structures and crystal chemistry in the system Na_{1+x}Zr₂Si_xP_{3-x}O₁₂. **1976**, *11* (2), 173-182.
56. Anantharamulu, N.; Rao, K. K.; Rambabu, G.; Kumar, B. V.; Radha, V.; Vithal, M. J. J. o. m. s., A wide-ranging review on Nasicon type materials. **2011**, *46* (9), 2821-2837.
57. Samiee, M.; Radhakrishnan, B.; Rice, Z.; Deng, Z.; Meng, Y. S.; Ong, S. P.; Luo, J. J. J. o. P. S., Divalent-doped Na₃Zr₂Si₂PO₁₂ natrium superionic conductor: Improving the ionic conductivity via simultaneously optimizing the phase and chemistry of the primary and secondary phases. **2017**, *347*, 229-237.
58. Vogel, E.; Cava, R. J.; Rietman, E. J. S. S. I., Na⁺ ion conductivity and crystallographic cell characterization in the Hf-nasicon system Na_{1+x}Hf₂Si_xP_{3-x}O₁₂. **1984**, *14* (1), 1-6.
59. Aono, H.; Sugimoto, E.; Sadaoka, Y.; Imanaka, N.; Adachi, G.-y. J. S. S. I., Electrical property and sinterability of LiTi₂(PO₄)₃ mixed with lithium salt (Li₃PO₄ or Li₃BO₃). **1991**, *47* (3-4), 257-264.
60. Sakuda, A.; Hayashi, A.; Takigawa, Y.; Higashi, K.; Tatsumisago, M. J. J. o. t. C. S. o. J., Evaluation of elastic modulus of Li₂S-P₂S₅ glassy solid electrolyte by ultrasonic sound velocity measurement and compression test. **2013**, *121* (1419), 946-949.
61. Takada, K.; Kondo, S. J. I., Lithium ion conductive glass and its application to solid state batteries. **1998**, *4* (1-2), 42-47.
62. Seino, Y.; Ota, T.; Takada, K.; Hayashi, A.; Tatsumisago, M. J. E.; Science, E., A sulphide lithium super ion conductor is superior to liquid ion conductors for use in rechargeable batteries. **2014**, *7* (2), 627-631.

63. Dirican, M.; Yan, C.; Zhu, P.; Zhang, X. J. M. S.; Reports, E. R., Composite solid electrolytes for all-solid-state lithium batteries. **2019**, *136*, 27-46.
64. Liu, X.; Li, X.; Li, H.; Wu, H. B. J. C. A. E. J., Recent Progress of Hybrid Solid-State Electrolytes for Lithium Batteries. **2018**, *24* (69), 18293-18306.
65. Keller, M.; Varzi, A.; Passerini, S. J. J. o. P. S., Hybrid electrolytes for lithium metal batteries. **2018**, *392*, 206-225.
66. Cheng, X.-B.; Zhao, C.-Z.; Yao, Y.-X.; Liu, H.; Zhang, Q. J. C., Recent advances in energy chemistry between solid-state electrolyte and safe lithium-metal anodes. **2019**, *5* (1), 74-96.
67. Li, S.; Zhang, S. Q.; Shen, L.; Liu, Q.; Ma, J. B.; Lv, W.; He, Y. B.; Yang, Q. H., Progress and Perspective of Ceramic/Polymer Composite Solid Electrolytes for Lithium Batteries. *Adv Sci (Weinh)* **2020**, *7* (5), 1903088.
68. Lim, Y. J.; Kim, H. W.; Lee, S. S.; Kim, H. J.; Kim, J.-K.; Jung, Y.-G.; Kim, Y., Ceramic-Based Composite Solid Electrolyte for Lithium-Ion Batteries. *ChemPlusChem* **2015**, n/a-n/a.
69. Choi, H.; Kim, H. W.; Ki, J.-K.; Lim, Y. J.; Kim, Y.; Ahn, J.-H., Nanocomposite quasi-solid-state electrolyte for high-safety lithium batteries. *Nano Research* **2017**, *10* (9), 3092-3102.
70. Kim, J.-K.; Lim, Y. J.; Kim, H.; Cho, G.-B.; Kim, Y., A hybrid solid electrolyte for flexible solid-state sodium batteries. *Energy Environ. Sci.* **2015**, *8* (12), 3589-3596.
71. Sun, C.; Liu, J.; Gong, Y.; Wilkinson, D. P.; Zhang, J. J. N. E., Recent advances in all-solid-state rechargeable lithium batteries. **2017**, *33*, 363-386.
72. Zhang, B.; Tan, R.; Yang, L.; Zheng, J.; Zhang, K.; Mo, S.; Lin, Z.; Pan, F. J. E. S. M., Mechanisms and properties of ion-transport in inorganic solid electrolytes. **2018**, *10*, 139-159.
73. Xue, Z.; He, D.; Xie, X. J. J. o. M. C. A., Poly (ethylene oxide)-based electrolytes for lithium-ion batteries. **2015**, *3* (38), 19218-19253.
74. Quartarone, E.; Mustarelli, P. J. C. S. R., Electrolytes for solid-state lithium rechargeable batteries: recent advances and perspectives. **2011**, *40* (5), 2525-2540.
75. Long, L.; Wang, S.; Xiao, M.; Meng, Y. J. J. o. M. C. A., Polymer electrolytes for lithium polymer batteries. **2016**, *4* (26), 10038-10069.
76. Pan, Q.; Smith, D. M.; Qi, H.; Wang, S.; Li, C. Y. J. A. M., Hybrid electrolytes with controlled network structures for lithium metal batteries. **2015**, *27* (39), 5995-6001.
77. Lin, D.; Liu, W.; Liu, Y.; Lee, H. R.; Hsu, P.-C.; Liu, K.; Cui, Y. J. N. I., High ionic conductivity of composite solid polymer electrolyte via in situ synthesis of monodispersed SiO₂ nanospheres in poly (ethylene oxide). **2016**, *16* (1), 459-465.
78. Lin, Y.; Wang, X.; Liu, J.; Miller, J. D. J. N. E., Natural halloysite nano-clay electrolyte for advanced all-solid-state lithium-sulfur batteries. **2017**, *31*, 478-485.

79. Liu, W.; Liu, N.; Sun, J.; Hsu, P.-C.; Li, Y.; Lee, H.-W.; Cui, Y. J. N. I., Ionic conductivity enhancement of polymer electrolytes with ceramic nanowire fillers. **2015**, *15* (4), 2740-2745.
80. Shim, J.; Kim, H. J.; Kim, B. G.; Kim, Y. S.; Kim, D.-G.; Lee, J.-C. J. E.; Science, E., 2D boron nitride nanoflakes as a multifunctional additive in gel polymer electrolytes for safe, long cycle life and high rate lithium metal batteries. **2017**, *10* (9), 1911-1916.
81. Commarieu, B.; Paoletta, A.; Daigle, J.-C.; Zaghbi, K. J. C. O. i. E., Toward high lithium conduction in solid polymer and polymer–ceramic batteries. **2018**, *9*, 56-63.
82. Zheng, J.; Tang, M.; Hu, Y. Y. J. A. C. I. E., Lithium ion pathway within Li₇La₃Zr₂O₁₂-polyethylene oxide composite electrolytes. **2016**, *55* (40), 12538-12542.
83. Zheng, J.; Hu, Y.-Y. J. A. a. m.; interfaces, New insights into the compositional dependence of Li-Ion transport in polymer–ceramic composite electrolytes. **2018**, *10* (4), 4113-4120.
84. Zagórski, J.; López del Amo, J. M.; Cordill, M. J.; Aguesse, F.; Buannic, L.; Llordés, A. J. A. A. E. M., Garnet–Polymer Composite Electrolytes: New Insights on Local Li-Ion Dynamics and Electrodeposition Stability with Li Metal Anodes. **2019**, *2* (3), 1734-1746.
85. Zhai, H.; Xu, P.; Ning, M.; Cheng, Q.; Mandal, J.; Yang, Y. J. N. I., A flexible solid composite electrolyte with vertically aligned and connected ion-conducting nanoparticles for lithium batteries. **2017**, *17* (5), 3182-3187.
86. Wang, X.; Zhai, H.; Qie, B.; Cheng, Q.; Li, A.; Borovilas, J.; Xu, B.; Shi, C.; Jin, T.; Liao, X. J. N. E., Rechargeable solid-state lithium metal batteries with vertically aligned ceramic nanoparticle/polymer composite electrolyte. **2019**, *60*, 205-212.
87. May, C., *Epoxy resins: chemistry and technology*. Routledge: 2018.
88. Suzuki, Y.; Kami, K.; Watanabe, K.; Watanabe, A.; Saito, N.; Ohnishi, T.; Takada, K.; Sudo, R.; Imanishi, N. J. S. S. I., Transparent cubic garnet-type solid electrolyte of Al₂O₃-doped Li₇La₃Zr₂O₁₂. **2015**, *278*, 172-176.
89. Xie, H.; Li, Y.; Goodenough, J. B. J. R. A., NASICON-type Li_{1+2x}Zr_{2-x}Ca_x(PO₄)₃ with high ionic conductivity at room temperature. **2011**, *1* (9), 1728-1731.
90. McENTIRE, B. J.; Bartlett, R.; Miller, G.; Gordon, R. J. J. o. t. A. C. S., Effect of decomposition on the densification and properties of nasicon ceramic electrolytes. **1983**, *66* (10), 738-742.
91. Sudheer, M.; Pradyoth, K.; Somayaji, S. J. A. J. o. M. S., Analytical and Numerical validation of epoxy/glass structural composites for elastic models. **2015**, *5* (3C), 162-168.

All the glory to God who helped me to complete this academic process. Thanks to Prof. Youngsik Kim, who led me to the Ph.D. course. Dedicate this dissertation to my father, Eun Sung Lim and my mother, Jeom Oak Bae and dear wife, Jung Min Lim, who have devoted and generously supported my education.